Planet migration in evolving protoplanetary discs

Linn Eriksson

Lund Observatory
Lund University

2018-EXA134

Degree project of 60 higher education credits (for a degree of Master)
May 2018

Supervisor: Anders Johansen

Lund Observatory
Box 43
SE-221 00 Lund
Sweden

Abstract

The rate of migration and accretion onto protoplanets is greatly influenced by the structure of the surrounding protoplanetary disc. This structure changes with time as the disc evolves on a million year timescale, implying that the process of planet formation might look very different depending on when it was initiated. Further on, the evolution of the disc structure is affected on smaller timescales by the presence of the planet, the most obvious effect being the planetary induced gap. In this project I will determine how much planet formation affects disc evolution. To do so I perform 1D simulations of an evolving viscous disc that is perturbed by an embedded planet that migrates and accretes gas. I will consider different models for migration and gas accretion, and compare the results to observations of protoplanetary discs with the ALMA telescopes. From the results I can confirm what was previously known, namely that 1D simulations yield deeper and narrower planetary gaps than their higher dimensional counterparts. The removal of gas from the disc due to gas accretion onto the planet significantly alters the final mass and semimajor axis of the planet. From my simulations I also find that the classical Type-I and Type-II migration scenario results in that most planets migrate to the inner edge of the protoplanetary disc. This can be avoided using a new migration model where the planets never enter into the Type-II regime, but continue to migrate under the actions of disc torques that are decreased by the opening of the planetary gap. In this scenario planets that start to accrete gas close to the star will migrate a short distance and then continue to accrete gas practically in-situ, while planets that start to accrete gas further out in the disc will migrate a longer distance before the migration halts.

Acknowledgments

I wish to thank my supervisor Anders Johansen for coming up with an interesting project which covers many topics of planet formation, and has given me a good idea of how research in astronomy is being done. Even more I wish to thank Anders for the opportunity to continue to work within this area of research in my upcoming PhD. I am grateful to Michiel Lambrechts for informative discussions regarding the pebble isolation mass, and to Bertram Bitsch for answering many questions about planet formation in general. I wish to thank Ross Church and Henrik Jönsson for their constructive feedback which led to an improved thesis. Last I wish to thank the people at the department who have given me the opportunity to develop as a researcher by not only publishing papers, but also talking about them at both informal meetings and at the For All conference in Lund.

Populärvetenskaplig beskrivning

En nyfödd stjärna är omgiven av en disk som består till mestadels av gas med en liten andel grus, en så kallad protoplanetarisk disk. Det är i den här disken som planeter bildas, och likt planeter så roterar den runt solen. En viktig egenskap hos den protoplanetariska disken är att den förändras med tiden. Stjärnans gravitation drar till sig material från disken, vilken gör att den blir mindre och mindre massiv ju längre tiden går. Samtidigt kommer strålning från stjärnan att värma gasen i disken och få topplagret att avdunsta. Dessa två processer gör att all gas i disken har försvunnit efter bara några miljoner år.

Några miljoner år är en väldigt kort period om man jämför med åldern på solsystemet, och under den här tiden måste alla planeter som består till största del utav gas hinna bildas. Sådana planeter kallas för gasjättar, och ett exempel på en gasjätte är Saturnus. Saturnus består av en fast kärna som är omgiven av en enorm mängd gas. Massan av Saturnus kärna är ungefär 10 gånger större än Jordens massa, och massan av gasen som omger den är hela 85 gånger större än Jordens massa. Denna jätteplanet måste alltså bildas på bara några miljoner år. Hur detta sker är fortfarande inte helt förstått. De steg som är involverade är: 1) gruskorn som kolliderar med varandra, fastnar och bildar småsten; 2) Om densiteten av småsten någonstans i disken blir tillräkligt hög så kan gravitationen binda ihop dem till asteriod-liknande objekt; 3) De största av dessa objekten fortsätter att växa genom att dra till sig mindre objekt; 4) Om dessa blir tillräkligt stora kan de börja dra till sig gas och utvecklas till gasjättar. I mitt projekt kommer jag att undersöka det sista steget, hur en planetkärna drar till sig gas.

Under tiden som planeten bildas kommer den att röra sig radiellt (migrera) genom disken. Till exempel, om en planetkärna bildas långt ut i disken vid Neptunus och Uranus, så kanske den befinner sig vid Jupiter när den har vuxit klart. Migration av planeter är ett stort problem inom planetformation, eftersom de flesta migrationsmodellerna vi har leder till att planeterna vandrar alldeles för snabbt och blir uppätna av stjärnan. I mitt projekt kommer jag att undersöka en ny modell för planetmigration som gör att planeterna inte blir uppätna av stjärnan.

Eftersom planeter bildas i disken, och eftersom allt material som de är uppbyggda av kommer ifrån den, så kommer planeterna att påverkas mycket av hur disken ser ut. Men kan planeterna påverka disken? Radioteleskopet ALMA, som består av 66 stora samarbetande teleskop, har lyckats ta bilder på ett antal protoplanetariska diskar. Diskarna på dessa bilder har mörka ringar i sig. Man tror att dessa ringar bildas av att planeter puttar bort material från sin bana när de roterar i disken. Planeterna gräver alltså ett hål i disken när de bildas, och ju mer massiv en planet är, desto djupare blir hålet. Alltså kan planeterna påverka disken på minst ett sätt, och hur stor denna påverkan är, är ytterligare en sak som jag kommer att undersöka.

Contents

Chapter 1

Introduction

Protoplanetary discs form around newly born stars and evolve on million year timescales as matter is accreted onto the central star (e.g. Haisch et al. 2001; Fedele et al. 2010). The lifetime of protoplanetary discs is constrained by finding the observed fraction of stars that has discs around them within a star forming cluster, as a function of the cluster age (see left panel of Figure 1.1). These observations suggest that 50% of the stars have lost their discs already after 3 Myr. The mass accretion rate onto the star has been loosely constrained from observations of accretion luminosities of accreting young stellar objects (Hartmann et al., 1998; Manara, 2014; Sicilia-Aguilar et al., 2010). For stellar ages between 1-3 Myr there are inferred mass accretion rates in the range between 10^{-10}-10^{-7} $M_\odot$/yr (see right panel of Figure 1.1). In the commonly used model of Hartmann (2009) (black line in Figure 1.1) the mass accretion rate decreases from 10^{-7} $M_\odot$/yr to around 10^{-8} $M_\odot$/yr in 3 Myr. Mass accretion onto the central star is made possible via a transfer of angular momentum outwards in the disc (Pringle, 1981). Because of this outward transfer of angular momentum, the disc expands with time (Lynden-Bell & Pringle 1974; Hartmann et al. 1998). Such a disc is called a *viscous accretion disc*, and it is often modeled using a 1-D approach where the column density evolves due the outwards transport of angular momentum.

Previous observations of thermal emission from dust at mm and cm wavelengths in protoplanetary discs have put constraints on their structure and lifetime. With the construction of ALMA (the Atacama Large Millimeter / submillimeter Array) observations of discs showing detailed structures such as rings and gaps has been made possible (e.g. ALMA Partnership et al. 2015; Fedele et al. 2017, 2018, see Figure 1.2). Various processes have been suggested to be the origin of such gap- and ring-structures, for example dust growth (Zhang et al., 2015; Okuzumi et al., 2016) and disc-planet interactions (e.g. Kanagawa et al. 2015b), but so far it has been difficult to establish the dominant process from the observations. By using simulations as well, this can be determined by modeling the different processes and comparing the resulting gap structures to observations. Further on, finding a relationship between the gap structure and the mass and size of a planet would put even stronger constraints on the planet formation process.

Protoplanets in the disc grow via the accretion of solids and gas in their vicinities.

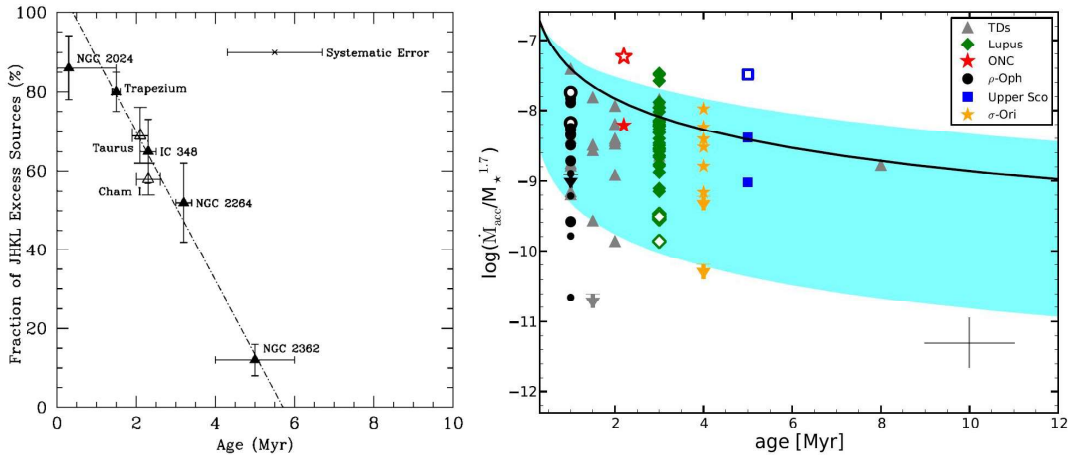

Figure 1.1: Left panel: fraction of stars within a star forming cluster that have discs around them, as a function of cluster age (Haisch et al., 2001). From this plot we learn that 50% of the stars have lost their discs after 3 Myr. Right panel: mass accretion rates as a function of stellar age (Manara, 2014). The different symbols represent observations in different star forming regions. The cyan region are values which can be reproduced by viscous evolution. The black line is the evolution model of Hartmann (2009).

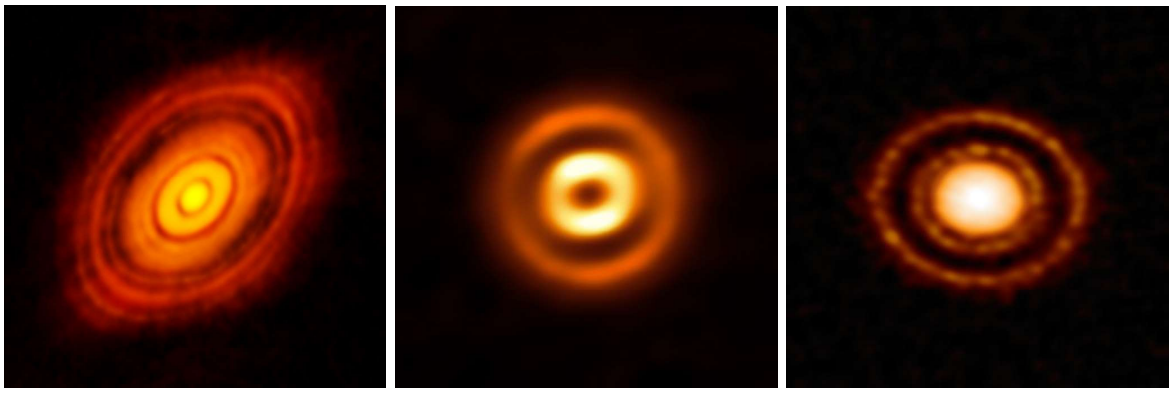

Figure 1.2: Observations at 1.3mm of (left panel) the protoplanetary disc around around HL Tau (ALMA Partnership et al., 2015), (middle panel) the protoplanetary disc HD 169142 (Fedele et al., 2017), and (right panel) the protoplanetary disc AS 209 (Fedele et al., 2018). The bright rings in the pictures appears due to emission from mm sized dust. In between these bright rings the density of mm sized dust is very low, we call these features gaps. One process which could explain these ring- and gap-structures in protoplanetary discs is planet formation.

There are two main theories describing the growth from planetesimals to solid planetary cores: planetesimal accretion and pebble accretion. For solar-like solid-to-gas ratios the first process alone takes a longer time than the lifetime of the disc itself (Pollack et al. 1996; Rafikov 2004; Levison et al. 2010). This problem can be remedied by including the accretion of mm-cm sized pebbles onto the protoplanet, a much faster process (Johansen & Lacerda 2010; Ormel & Klahr 2010; Lambrechts & Johansen 2012; Morbidelli & Nesvorny 2012). During the pebble accretion process, the protoplanet starts to attract a gaseous envelope. Heat generated when the pebbles fall down through the protoatmosphere provides pressure support to the gas envelope and hinders it from falling down onto the protoplanet. This flow of pebbles through the protoatmosphere halts at the so called *pebble isolation mass* (Lambrechts & Johansen, 2014; Bitsch et al., 2018), after this mass has been reached the gaseous envelope can start to contract onto the protoplanet. Subsequent gas accretion continues until the disc has been depleted of gas.

During the planet formation process there are important interactions taking place between the protoplanet and the surrounding gaseous disc, these are illustrated in Figure 1.3 for a protoplanet moving clockwise in a protoplanetary disc. The protoplanet's *coorbital region* divides the disc into an inner and outer part (middle panel). Exchange of angular momentum between the protoplanet and material that executes horseshoe turns relative to it (material in the coorbital region) gives rise to a *corotation torque*. The protoplanet further generates spiral density waves in the disc which gives rise to *Lindblad torques* (left panel) (Goldreich & Tremaine 1979, 1980). The inner spiral rotates ahead of the protoplanet and pulls it forward. By doing so it exerts a positive torque on the protoplanet which results in a gain of angular momentum and outward migration. On contrast, the outer spiral rotates behind the protoplanet and results in inward migration. The total torque acting on the planet is the sum of the Lindblad and the corotation torques, and will generally be directed inwards. For low mass protoplanets that do not significantly perturb the disc, a linear analysis of the Lindblad and corotation torque can be used to infer the orbital evolution of the protoplanet, resulting in what we call *Type-I migration*.

If a planet grows massive enough for the planetary torque to deplete the coorbital region, it results in an annular gap being carved around the planetary orbit (Lin & Papaloizou, 1986a). Since the density in the coorbital region is low the corotation torque becomes insignificant, and for large gaps even the Lindblad torque becomes suppressed by gap formation. Until not long ago it was the common belief that the planet becomes coupled to the viscous evolution of the disc at this point, and continues to migrate with what is called *Type-II migration*. In this picture the gas flowing through the protoplanetary disc will slowly pile up at the outer edge of the gap, strengthening the outer Lindblad torque and forcing the planet to migrate at the same speed as the viscous accretion speed of the gas. Recent studies of migration of gap-opening planets however show that this might not be the case (e.g. Duffell et al. 2014; Dürmann & Kley 2015). In order for the planet to become coupled to the viscous evolution of the disc, the disc must be split to an inner and outer part, and in order for that to occur gas must be prevented from flowing across the planetary gap. Duffell et al. (2014) show that gas can actually cross the gap, even for very deep gaps, and hence there should be no Type-II regime for migration. Dürmann &

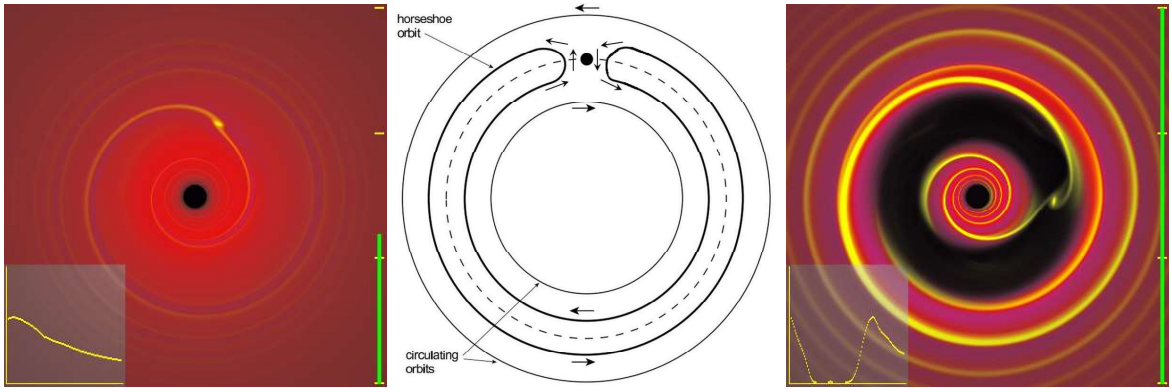

Figure 1.3: These plots from Armitage & Rice (2005) show the interaction between a protoplanetary disc and a planet that orbits clockwise in it. In the left panel the planet is of low mass and still embedded in the disc, this is called *Type-I migration*. In the right panel the planet has gained enough mass to open up a gap in the disc. In the classical migration picture no or little mass is allowed to cross the planetary gap at this stage, resulting in what is called *Type-II migration*. The middle panel shows a sketch of the streamlines close to the planetary orbit. The planets coorbital region divides the disc into an inner and outer part, and material inside the coorbital region executes horseshoe turns relative to the planet (the direction of motion is indicated by arrows in the figure).

Kley (2015) also investigated giant planet migration and found that the migration rate of a planet is entirely governed by the gravitational torque exerted on it by the disc, and thus completely independent of the viscous speed of the disc. Kanagawa et al. (2018) continued on this track and showed using 2-D hydrodynamical simulations that the torque on the planet is roughly proportional to the depth of the planetary gap. The migration of planets is still a very active area of research and as of today there are still new developments that can change our picture of migration substantially..

In this project I use 1D simulations to model the evolution of a viscous accretion disc that is being perturbed by a growing protoplanet. I will not model the formation of the planetary core, but instead start the protoplanets at their pebble isolation mass and consider the accretion of gas onto the core. Furthermore, I will test different models for planetary migration. The aim of this work is to determine the effect that planet formation has on disc evolution. I am particularly interested in finding any observational effects on the disc, which could help to connect planet formation models with observations of protoplanetary discs. The most obvious way in which a protoplanet affects the disc structure is by the formation of a planetary gap. I will compare gap depths produced in my 1D simulations to those of others, and investigate what effect the gap depths have on the gas accretion rates onto the planet, as well as the migration rates. I will then compare the resulting growth tracks to observations, in order to draw conclusions about the realism of the different models for gap opening, gas accretion and migration. I will show that (a) the new models for type-II migration yield growth tracks in good agreement with the

observations of dark rings in protoplanetary discs and (b) that inclusion of gas accretion has a significant effect on the observational properties of the protoplanetary disc.

Chapter 2

Background theory

In this chapter I will summarize all the different equations that are used in this work. For further details the reader is directed to the literature cited in the following sections. Protoplanetary discs form around young stars and evolve with time (Sect. 2.1) as matter is accreted onto the central star. It is inside such discs that the planet formation process takes place. Observations have shown a large diversity of planetary systems. For example, around 30% of all stars are expected to harbor a super-Earth (e.g. Fressin et al. 2013; Fulton et al. 2017), and Jupiter analogs have an inferred occurrence rate of around 3% (Rowan et al., 2016; Vigan et al., 2017). In this project I will limit myself to study the formation of gas giants, where by gas giants I refer to planets that reach their pebble isolation mass (Sect. 2.2), and thus start to accrete a gaseous envelope (Sect. 2.3). Such planets do not grow in-situ at a fixed radial distance from the star, but they migrate through the disc (Sect. 2.4) during the formation process.

2.1 Evolution of the disc structure with time

The surface density evolution of a viscous disc that is perturbed by a planet can be described by a one dimensional equation derived in Lin & Papaloizou (1986b),

$$\frac{\partial \Sigma}{\partial t} = \frac{1}{R}\frac{\partial}{\partial R}\left[3R^{1/2}\frac{\partial}{\partial R}(\nu \Sigma R^{1/2}) + \frac{2\Lambda \Sigma R^{3/2}}{(GM_*)^{1/2}}\right], \tag{2.1}$$

where Σ is the surface density, t is the time, R is the semimajor axis, ν is the kinematic viscosity of the disc, Λ is the torque density distribution, G is the gravitational constant, and M_* is the stellar mass. The torque density distribution is the rate of angular momentum transfer per unit mass, directed from the disc to the protoplanet. Note that this equation is derived assuming Keplerian rotation, $\Omega = (GM_*/R^3)^{1/2}$.

Equation (2.1) is essentially a form of the continuity equation in cylindrical coordinates,

$$\frac{\partial \Sigma}{\partial t} = -\frac{1}{R}\frac{\partial}{\partial R}(\Sigma v_{\rm R} R), \tag{2.2}$$

with two radial velocity components, $v_{\rm R} = v_{\rm R,viscous} + v_{\rm R,planet}$. The first term describes the viscous evolution of the disc, while the second governs the tidal effect of the protoplanet-disc interaction. The radial velocity components are obtained by simply dividing the terms in the square bracket in Eq. (2.1) by $(-\Sigma R)$, to obtain

$$v_{\rm R,viscous} = -\frac{3}{\Sigma R^{1/2}} \frac{d}{dR}(\nu \Sigma R^{1/2}), \tag{2.3}$$

$$v_{\rm R,planet} = -\frac{2\Lambda R^{1/2}}{\sqrt{GM_*}}. \tag{2.4}$$

While the viscous term governs the global radial velocity of gas in the disc, the planet induced term only affect the radial velocity of gas close to the planetary orbit. For a large planetary mass, which translates to a large torque density, gas in the vicinity of the planetary orbit will obtain large radial velocities and move away from the planet, thus creating a gap. In the case of a multiple-planet system each planet contributes a torque density distribution to the second term.

The kinematic viscosity of the disc is approximated using the standard α approach of Shakura & Sunyaev (1973), $\nu = \alpha \Omega H^2$, where α is a parameter roughly between 0 and 1 that determines the efficiency of turbulent momentum transport, and H is the disc scale height. I adopt the scale height

$$H = \frac{c_s}{\Omega}, \tag{2.5}$$

where c_s is the sound-speed, calculated as

$$c_s = \left(\frac{kT}{\mu m_H}\right)^{1/2} = 9.9 \times 10^4 \left(\frac{2.34}{\mu}\frac{T}{280}\right)^{1/2} \text{cm s}^{-1}. \tag{2.6}$$

Here μ is the mean molecular weight, which I set to be 2.34 for a cosmic mixture of hydrogen and helium (Hayashi, 1981). The temperature structure of the disc is approximated as

$$T = \mathrm{T}_{\rm 1au} \times R^{-\zeta} (L/L_\odot)^{1/4} \mathrm{K}, \tag{2.7}$$

where $\mathrm{T}_{\rm 1au}$ is the temperature in the midplane of the disc at 1 au, and ζ sets the slope of the temperature with radius (Hayashi, 1981). The standard temperature exponent used in this thesis is $\zeta = 3/7$, and the temperature at 1 au is set to be 150 K. These values are derived from models of passive discs, where one only considers stellar heating (Chiang & Goldreich, 1997).

The radial mass flux across the disc, which will be referred to as the "disc accretion rate", is simply

$$\dot{M} = 2\pi R \Sigma (-v_{\rm R}), \tag{2.8}$$

where the minus sign originates from the convenction that $\dot{M} > 0$ when $v_{\rm R} < 0$ (Pringle, 1981). As can be seen in the right panel of Figure 1.1, the disc accretion rate decreases with time, and the decrease is non-linear. In viscous evolution models the decrease in disc

accretion rate is set by the size of the disc and α. Hartmann et al. (1998) represent this decline as $\dot{M} \propto t^{-\eta}$, and estimate η to be between 1.5 and 2.8.

As mentioned in the introduction, mass accretion onto the star is made possible via a transfer of angular momentum outwards in the disc. This raises the question of what drives this angular momentum transport in protoplanetary discs? In the standard picture, the disc viscosity is driven by turbulence that arises when ionized atoms and molecules hit the disc and interact with the magnetic fields within it, referred to as MRI (magnetorotational instability, see Balbus & Hawley 1991). MRI is a linear instability which occurs because an ideal magnetohydrodynamic (MHD) flow is stable only if the angular velocity increases with radius. This is not satisfied in Keplerian discs, and thus sufficiently well-ionized discs are rendered unstable. However, in order for this mechanism to work efficiently there must be enough ions in the gas, and it has been suggested that the ionization fraction in protoplanetary discs may become quite low (e.g. Umebayashi & Nakano 1988; Gammie 1996).

Ionization of atoms and molecules occurs mainly due to cosmic-rays and X-rays hitting the protoplanetary disc. Such processes are most efficient in the top-layer of the disc, and thus the level of ionization varies between different parts of the disc. The mid-plane of the disc, which is more or less shielded from such rays, suffers a lower degree of ionization and is therefore MRI inactive. This has been dubbed the "dead zone" in protoplanetary discs (Gammie, 1996; Sano et al., 2000). Pinte et al. (2016) compared models of dust emission from protoplanetary discs to ALMA observations of the disc surrounding HL Tau (see left panel of Figure 1.2). They found that in order to match the observed accretion rate onto the star $\alpha \sim 10^{-2}$ was required; however, for modeling dust settling to the mid-plane they found that observations are consistent with $\alpha \sim 10^{-4}$ for the turbulent diffusion of dust particles. This could either be explained by that different physical mechanisms control the viscous and the diffusive alpha, and/or that α varies radially within the disc (as in the case when there is a dead zone).

Another mechanism that could drive the viscous evolution of the disc is magnetically-coupled disc winds (Bai & Stone, 2013; Turner et al., 2014), which carry angular momentum along the magnetic field lines in the disc, causing it to lose angular momentum. In this work I will not separate different physical mechanisms for driving turbulence. Instead I will choose an α for disc accretion which is consistent with observations, and when possible a reduced α in the mid-plane of the disc which is similar to the one suggested for HL Tau, and produces reasonable gas accretion rates onto the planetary core.

2.1.1 Torque density distributions

Planets excite density waves through gravitational interactions with the surrounding disc (see e.g. Goldreich & Tremaine 1980). These density waves carry angular momentum away from the planet. Due to gradual wave-dampening, caused by the disc viscosity or non-linear steepening (e.g. Lin & Papaloizou 1986b), this angular momentum is deposited on the disc. Therefore, the planet exerts a torque on the disc material.

The deposition of angular momentum on the disc as caused by the planet is the direct

cause of gap-formation; however, modeling this requires detailed hydrodynamical simulations. One common way to simplify this problem is to remove the gap-forming planet, and instead apply a torque on the disc. This torque now becomes the mechanism of gap-formation; however, it is important to remember that the applied torque only is an approximation to the presence of a real planet. In order to calculate Eq. (2.1) one needs to specify the functional form of Λ, which depends on where in the disc angular momentum is deposited. In this work I will assume instantaneous wave-dampening. The credibility of this approximation will be discussed in further detail in chapter 4.2; but generally, if the kinematic viscosity is relatively large then the dissipation will be concentrated in the vicinity of the planet's orbit, making it a reasonable approximation (Papaloizou & Lin, 1984).

The angular momentum exchange between a protoplanetary disc and a protoplanet, or analogously that between binary stars and accretion discs, has been calculated by various methods. One common way to model Λ would be to use the impulse approximation of Lin & Papaloizou (1986b),

$$\Lambda = \text{sign}(R-a)\frac{fq^2GM_*}{2R}\left(\frac{R}{|\Delta_0|}\right)^4, \tag{2.9}$$

where the torque on the planet has been calculated approximately by considering the exchange of angular momentum between a planet and individual particles passing by it. In the above equation a is the semimajor axis of the protoplanet, f is a dimensionless constant, q is the planet to star mass ratio, and Δ_0 is taken to be the maximum of H or $|R-a|$. Although this is a commonly used form of Λ, which has been proved to match results obtained from summing over Lindblad resonances (see e.g. Goldreich & Tremaine 1980), it comes with sharp transitions in the profile and has a long tail that is unphysical (see e.g. D'Angelo & Lubow 2010 and references therein).

D'Angelo & Lubow (2010) provide an improved 1D description for Λ, which shows better agreement to hydrodynamical simulations including a planet than the impulse approximation. The equation they provide is

$$\Lambda = -F(x,\beta,\xi)\Omega_a^2 a^2 q^2\left(\frac{a}{H_a}\right)^4, \tag{2.10}$$

where F is a dimensionless function, $x = (R-a)/H_a$, $\beta = -\frac{\partial \ln \Sigma}{\partial \ln r}$ and $\xi = -\frac{\partial \ln T}{\partial \ln R}$. This is the torque density distribution that I will use to model gap-formation in this work. Equation (2.10) describes the torque density exerted on the planet by the disc, and includes contributions from both Lindblad resonances and the corotational resonance. Prior to D'Angelo & Lubow (2010) the function F was taken to be an inverse power law with distance from the planet that was modified close to the planet. One of the improvements that they introduced was to find a more accurate analytic expression for F by fitting the results of 3D simulations. The functional form of F used for fitting is

$$F(x,\beta,\xi) = \left\{p_1\exp\left[-\frac{(x+p_2)^2}{p_3^2}\right] + p_4\exp\left[-\frac{(x+p_5)^2}{p_6^2}\right]\right\}\times\tanh(p_7 - p_8 x) \tag{2.11}$$

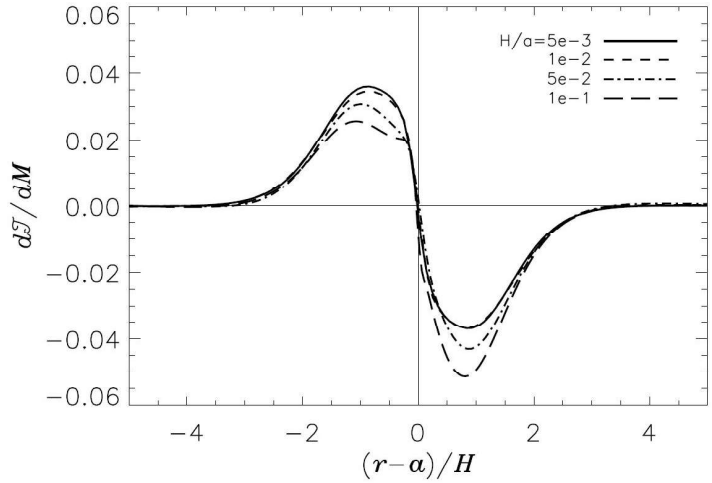

Figure 2.1: Figure adapted from D'Angelo & Lubow (2010). Torque density distribution for different values of the scale height at the planets location. This plot was produced using $\beta = 0.5$ and $\xi = 1$. The torque density is scaled by the quantity $\Omega_a^2 a^2 q^2 \left(\frac{a}{H_a}\right)^4$.

where $(p_1, \ldots, p_8)$ are parameters resulting from the fit. The tanh part affects the slope with which the profile goes from positive to negative. D'Angelo & Lubow (2010) has a table of parameters for specific values of β and ξ, which I will interpolate between in order to obtain a good fit for the function F.

Equation (2.10) is derived under the assumption that the mass density distribution along the orbit of the planet remains largely unperturbed. When the tidal torque of the planet exceeds the viscous torque responsible for disc spreading, this criterion breaks down and a gap is formed. D'Angelo & Lubow (2010) find that gap-opening planets introduce variations to the height of the peak in the torque density distribution of a factor around 2-3. Therefore, they introduce a factor of 1/2 to Eq. (2.10) for cases when the tidal torque exceeds the viscous torque. I will also use this extra factor when the Hill radius of the planet exceeds the disc scale height at the planet's location. I will then exchange the term $\left(\frac{a}{H_a}\right)^4$ with $\left(\frac{a}{r_H}\right)^4$ in Eq. (2.10), where r_H is the Hill radius. Furthermore, D'Angelo & Lubow (2010) tested the universality of function F to changes in α, q and H/a. They obtain very small variations for changes in α and q; however, the variation they obtain from changing H/a is more significant (see Figure 2.1 which is the same as Figure 3 in D'Angelo & Lubow (2010)).

2.2 Pebble isolation mass

The pebble isolation mass M_{iso} is the mass at which pebble accretion is halted and gas accretion can initiate. In the following section I will explain what causes the flow of pebbles to stop at this mass, and how it can be derived.

The pressure P in the midplane of an unperturbed disc, which is proportional to $\Sigma T/H$, decreases outwards. This negative pressure gradient results in a pressure force directed away from the star. Pebbles, which are not supported by pressure, would continue to orbit at the Keplerian velocity, set by the balance between the gravitational acceleration towards the star and the centripetal force directed outwards in the disc. This is not the case for the gaseous component of the disc. Since gas is supported by pressure and therefore feels the effect of this outward pressure force, the centripetal force does not have to be as large in order to remain at the same orbit and conserve angular momentum. Therefore the gas component of the disc will orbit at sub-Keplerian velocity. The pebbles therefore feel a headwind due to the sub-Keplerian velocity of the gas, and subsequently lose angular momentum and spiral inwards. This is what causes the radial drift of the pebbles in discs. The velocity difference between the gaseous component of the disc and the Keplerian motion can be described as

$$v_{\text{gas}} = v_{\text{K}}(1-\eta) = v_{\text{K}} - \eta v_{\text{K}} = v_{\text{K}} - \Delta v \tag{2.12}$$

where

$$\eta = -\frac{1}{2}\left(\frac{H}{r}\right)^2 \frac{\partial \ln P}{\partial \ln r} \tag{2.13}$$

(Nakagawa et al., 1981; Bitsch et al., 2018).

As long as the radial pressure gradient in the disc is negative, pebbles will continue to drift towards the star. Globally this will always be the case in protoplanetary discs; however, if there are gap-opening protoplanets in the disc, they can change the sign of the radial pressure gradient locally. When a gap is opened up it creates a positive radial surface density gradient just outside the orbit of the protoplanet. If $\frac{d\ln\Sigma}{d\ln R} > \frac{d\ln T}{d\ln R} - \frac{d\ln H}{d\ln R}$, it will generate a pressure maximum outside the planetary orbit. This will cause the gas to orbit at super-Keplerian velocity in a ring just outside the orbit of the planet. At this location in the disc, pebbles will feel a net outward acceleration, and instead of radially drifting over the planetary orbit they will pile up outside the planet. At these locations the density of pebbles can become large enough to trigger planetesimal formation, and by doing so aiding the formation of other planets.

The pebble isolation mass is defined as the mass where the velocity of the gas equals the Keplerian velocity. This occurs at $\eta = 0$, see equations 2.12 and 2.13, which is equivalent to $\partial \ln P/\partial \ln r = 0$. This criterion can in turn be written as

$$\frac{d\ln P}{d\ln R} = \frac{d\ln(\Sigma T/H)}{d\ln R} = \frac{d\ln\Sigma}{d\ln R} + \frac{d\ln T}{d\ln R} - \frac{d\ln H}{d\ln R}. \tag{2.14}$$

The logarithm of the radial surface density and temperature gradients are respectively $-\beta$ and $-\zeta$, and the scale height depends on R as

$$H = \frac{c_s}{\Omega_K} \propto \frac{T^{1/2}}{R^{-3/2}} \propto \frac{R^{-\zeta/2}}{R^{-3/2}} = R^{\frac{3-\zeta}{2}}. \tag{2.15}$$

From this I finally drive the logarithmic derivative of the pressure gradient as

$$\frac{d\ln P}{d\ln R} = -\beta - \zeta - \frac{3-\zeta}{2} = -\beta - \left(\frac{\zeta+3}{2}\right). \tag{2.16}$$

Since in this work I will use a constant temperature profile, the pebble isolation mass is obtained by finding the planetary mass at which $\beta = -\left(\frac{\zeta+3}{2}\right)$.

Bitsch et al. (2018) derive an analytical fitting formula for the pebble isolation mass using 3-D hydrodynamic simulations of planet-disc interactions. As in this work, they use a radial temperature profile that is constant throughout the simulation, and find the planetary mass at which $\eta = 0$. They further investigate how the pebble isolation mass scales with disc aspect ratio, viscosity and global radial pressure gradient. They obtain this way the fit

$$M_{\rm iso} = 25 \times f_{\rm fit} \mathrm{M}_{\oplus} \tag{2.17}$$

where

$$f_{\rm fit} = \left[\frac{H/R}{0.05}\right]^3 \left[0.34\left(\frac{\log(\alpha_3)}{\log(\alpha)}\right)^4 + 0.66\right]\left[1 - \frac{\frac{\partial \ln P}{\partial \ln R} + 2.5}{6}\right], \tag{2.18}$$

where $\alpha_3 = 0.001$.

2.3 Gas accretion

During pebble accretion the protoplanet starts to attract gas from the disc; however, due to heat generated from pebbles raining down in the proto-atmosphere, the hot hydrostatic envelope contains a gas mass that is much smaller than the core mass. Until pebble isolation mass is reached and the flow of pebbles stops, the attracted gas will remain in a proto-envelope around the core. Even so, Lambrechts & Johansen (2014) and Bitsch et al. (2015b) argue that small amounts of highly polluted gas can become bound to the planet during pebble accretion. They assume a gas to solid ratio of 1:9, meaning that 10% of the mass is counted as gas prior to the pebble isolation mass is reached. I will make the same assumption, and since I do not model solid accretion, I will initiate the planets in my simulations at their pebble isolation mass.

I use two different models to calculate the gas accretion rates onto the planet. In the first model I follow Bitsch et al. (2015b) directly. After the pebble isolation mass has been reached, the proto-envelope starts to contract onto the core. Machida et al. (2010) performed 3-D hydrodynamical simulations and found that the gas accretion rate increases with planetary mass up to a certain critical mass, after which is saturates or decreases. Piso & Youdin (2014) show that this critical mass is reached roughly when the mass of the envelope equals the mass of the core. While $M_{\rm env} < M_{\rm core}$, the contraction takes place on a long timescale, leading to low gas accretion rates. Piso & Youdin (2014) estimated the contraction time of the proto-envelope, and from that Bitsch et al. (2015b) extracted the

corresponding gas accretion rate

$$\dot{M}_{\rm gas} = 0.00175 f^{-2} \left(\frac{\kappa_{\rm env}}{1\ {\rm cm}^2/{\rm g}}\right)^{-1} \left(\frac{\rho_c}{5.5\ {\rm g/cm}^3}\right)^{-1/6} \left(\frac{M_c}{\rm M_E}\right)^{11/3} \times \left(\frac{M_{\rm env}}{0.1\ \rm M_E}\right)^{-1} \left(\frac{T}{81\ \rm K}\right)^{-0.5} \frac{\rm M_E}{\rm Myr}. \tag{2.19}$$

In this equation f is a fudge factor, $\kappa_{\rm env}$ is the opacity in the gaseous envelope and ρ_c is the core density. The factor f is varied in order to match analytical and numerical results. I will adopt a value of 0.2 for f, similar to Piso & Youdin (2014). For the envelope opacity and core density I adopt the same values as in Bitsch et al. (2015b), $\kappa_{\rm env} = 0.05\ {\rm cm}^2/{\rm g}$ and $\rho_c = 5.5\ {\rm g/cm}^3$.

When the envelope mass grows larger than the core mass, the gas accretion rate saturates and is no longer dependent on the planetary mass. The gas accretion rate at this stage has been calculated by Machida et al. (2010) using 3-D hydrodynamical simulations, and are taken as the minimum of the following two accretion rates

$$\dot{M}_{\rm gas,low} = 0.83 \Omega \Sigma H^2 \left(\frac{r_{\rm H}}{H}\right)^{9/2} \tag{2.20}$$

and

$$\dot{M}_{\rm gas,high} = 0.14 \Omega \Sigma H^2. \tag{2.21}$$

These gas accretion rates are calculated using the unperturbed surface density at the location of the planet.

In the second model of gas accretion I will follow Tanigawa & Tanaka (2016). They argue that if sufficient gas is supplied towards the protoplanet's orbit by disc accretion, the gas accretion rate will be determined by the hydrodynamics of the gas flow onto the protoplanet, which they call $\dot{M}_{\rm p,hydro}$. This rate can be calculated using the following equation

$$\dot{M}_{\rm p,hydro} = D \Sigma_{\rm acc}, \tag{2.22}$$

where D is the area in which the gas is to be accreted onto the planet per unit time, and $\Sigma_{\rm acc}$ is the surface density at the accretion channel in the disc (Tanigawa & Tanaka, 2016). According to the results of 2D hydrodynamical simulations of the accretion flow onto a planet performed by Tanigawa & Watanabe (2002), D in the equation above is given by

$$D = 0.29 \left(\frac{H_a}{a}\right)^{-2} q^{4/3} a^2 \Omega_a. \tag{2.23}$$

Tanigawa & Tanaka (2016) did not use a torque density distribution to carve the planetary gap, instead they used an empirical formula for the gas surface density at the bottom of the gap. From hydrodynamical simulations Kanagawa et al. (2015) obtained the fit

$$\Sigma_{\rm acc} = \frac{1}{1 + 0.04K} \Sigma_{\rm unp}, \tag{2.24}$$

where

$$K = \left(\frac{H_a}{a}\right)^{-5} q^2 \alpha^{-1}. \tag{2.25}$$

In all my simulations of gas accretion where I use the model of Tanigawa & Tanaka (2016), I will use both gap depths produced in my own simulations and gap depths calculated using Eq. (2.24). Similar to Bitsch et al. (2015b) I limit the gas accretion rate to 80% of the disc accretion rate. This limitation comes from the fact that a planet can not accrete at a higher rate than the global gas flow in the disc can supply, and Lubow & D'Angelo (2006) predicted that the mass flow onto the star across the planetary gap is around 10-25% of the mass accretion rate outside the planetary orbit.

Since the gas that is accreted onto the planet comes from the disc, I will perform some simulations where I decrease the surface density within one hill radii from the planet by a corresponding amount. Because the effect on the disc is expected to be small, I will remove equal amounts of gas from each grid cell within one Hill radius, and neglect the fact that the grids are unequally spaced in R (see chapter 3).

2.4 Planet migration

The transfer of angular momentum in the disc causes the planet to migrate at a rate

$$\frac{\mathrm{da}}{\mathrm{dt}} = -\frac{1}{2\pi}\left(\frac{a}{GM_*}\right)^{1/2}\left(\frac{4\pi}{M_\mathrm{p}}\right)\Gamma, \tag{2.26}$$

where M_p is the planetary mass and

$$\Gamma = 2\pi \int \Lambda \Sigma R dR \tag{2.27}$$

is the total torque exerted on the planet (Lin & Papaloizou, 1986b). This equation has been derived from the conservation of total angular momentum. In this work I will apply different prescriptions for the total torque, and compare the resulting migration rates with each other. As a first simple approach for migration I will use a Type-I torque formula from D'Angelo & Lubow (2010),

$$\Gamma = -(1.36 + 0.62\beta + 0.43\xi) \times \Sigma_a \Omega_a^2 a^4 q^2 \left(\frac{a}{H}\right)^2, \tag{2.28}$$

which describes the total torque exerted on a low-mass planet that is still embedded in the disc. Since the gas disc is expected to be largely unperturbed, β is calculated using the unperturbed surface density profile. Since this torque formula does not include any dependence on the gap shape, it can only be used to compare migration rates of planets with mass up to a few tens of Earth masses.

As a second approach I will implement the same migration prescriptions as used in Bitsch et al. (2015b). The total torque acting on embedded planets is a sum of the Lindblad

torque $\Gamma_{\rm L}$ and the corotation torque $\Gamma_{\rm C}$. In Paardekooper et al. (2010) it was shown that the non-linear corotation torque, or horseshoe drag, is prone to saturation. In order to maintain the corotation torque both thermal diffusion and viscosity are needed. However, since the global α in my disc is fairly high, I choose to ignore the risk of saturation and instead work with the total unsaturated torque $\Gamma_{\rm tot}$. In this work $\Gamma_{\rm tot}$ is computed using a prescribed formula from Paardekooper et al. (2010). Similar to the Type-I torque formula from D'Angelo & Lubow (2010), the total unsaturated torque prescription from Paardekooper et al. (2010) depends on the local radial gradients of surface density and temperature. Furthermore, the total unsaturated torque also depends on the negative of the local radial gradient of entropy ϵ, which is related to β and ξ according to $\epsilon = \xi - (\gamma - 1)\beta$, where γ is the adiabatic index.

I will simply list the unsaturated torques here, for details on each one of them see Paardekooper et al. (2010). The Lindblad torque is

$$\gamma\Gamma_{\rm L}/\Gamma_0 = -2.5 - 1.7\xi + 0.1\beta, \tag{2.29}$$

the baryonic part of the horseshoe drag is

$$\gamma\Gamma_{\rm hs,baro}/\Gamma_0 = 1.1\left(\frac{3}{2} - \beta\right), \tag{2.30}$$

the entropy-related part of the horseshoe drag is

$$\gamma\Gamma_{\rm hs,ent}/\Gamma_0 = 7.9\frac{\epsilon}{\gamma}, \tag{2.31}$$

the baryonic part of the linear corotation torque is

$$\gamma\Gamma_{\rm c,lin,baro}/\Gamma_0 = 0.7\left(\frac{3}{2} - \beta\right), \tag{2.32}$$

and the entropy-related part of the linear corotation torque is

$$\gamma\Gamma_{\rm c,lin,ent}/\Gamma_0 = \left(2.2 - \frac{1.4}{\gamma}\right)\epsilon. \tag{2.33}$$

All torques are normalized to $\Gamma_0 = (q/h)^2\Sigma_a a^4\Omega_a^2$, where $h = H/R$ is the disc aspect ratio taken at the position of the planet. The total torque is obtained by adding the contributions from Eq. (2.29)-(2.33).

For massive gap-opening planets Bitsch et al. (2015b) consider a transition to the Type-II migration regime. The idea behind Type-II migration is that when a protoplanet grows massive enough to open up a deep gap, here defined as $\Sigma_{\rm gap} < 0.1\Sigma_{\rm g}$, the disc is split into two parts (in this equation $\Sigma_{\rm g}$ refers to the surface density of the unperturbed gas disc). When this criterion is fulfilled the protoplanet positions itself in the middle of the gap so that the transfer of angular momentum on both sides of it is precisely balanced. Since the protoplanet is locked in the middle of the gap, it will continue to migrate with the

viscous accretion speed of the disc, which can be significantly slower than Type-I migration, particularly if α is low. The viscous accretion timescale of the disc is $\tau_\nu = a^2/\nu$, where the timescale is defined as $\tau = a/\dot{a}$. The migration speed can be further reduced if the planet grows much more massive than the gas outside the gap. This occurs if $M_\mathrm{p} > 4\pi\Sigma a^2$ and results in Type-II migration timescales of

$$\tau_\mathrm{II} = \tau_\nu \times \max\left(1, \frac{M_\mathrm{p}}{4\pi\Sigma a^2}\right) \tag{2.34}$$

(Baruteau et al., 2014). In this work I will allow a sharp transition between Type-I and Type-II migration, in contrast to the smooth transition used in Bitsch et al. (2015b).

As discussed in the introduction, whether or not Type-II migration exists is a disputed subject. If gas is allowed to cross the planetary gaps even for high-mass planets, there will be no separation between the inner and outer disc, and thus no Type-II migration. Dürmann & Kley (2015) reach the conclusion that planetary migration is entirely determined by the disc torques acting on the planet, and thus completely independent of the viscous timescale. Since the regions close to a gap-opening planet are mostly depleted of mass, they will not exert a significant torque onto the planet. This is confirmed by Kanagawa et al. (2018), where they also use 2-D hydrodynamical simulations to show that the torque on the planet is roughly proportional to the gap depth. Based on this result I construct a migration model where I use Type-I torques of Paardekooper et al. (2010) and replace the unperturbed surface density by the perturbed surface density at the position of the planet. This will result in migration rates which are proportional to the depth of the planetary gap, as suggested by Kanagawa et al. (2018).

As the final approach for migration I will let the planets migrate self-consistently under the action of the same torque density distribution that is used for the planetary gaps. Since Eq. (2.10) includes contributions from both Lindblad and corotation resonances, it should readily be able to describe the migration of planets, which D'Angelo & Lubow (2010) also confirmed in their paper. I will not do a transition to Type-II migration, but use this torque also for gap-opening planets. The biggest difference between this migration model and the previous one is that the migration rate now is proportional to the radial integral of the perturbed surface density, and not directly proportional to the gap depth.

Chapter 3

Numerical methods

I have written a code in Fortran 90 that solves the surface density evolution of a viscous accretion disc, and if present, the evolution of the orbit and mass of a protoplanet. The code is modularized and allows the user to easily determine what set of initial conditions and parameters to use for the disc and the protoplanet, as well as which output files to produce.

I solve Eq. (2.1) numerically using a first order finite difference scheme. I use the trick from Pringle et al. (1986) and solve the equation on a grid of points that are equally spaced in $R^{1/2}$. By using a radial variable $X = 2R^{1/2}$ and dependent variables $S = \frac{1}{8}X^3\Sigma$ and $V = \frac{3}{2}\nu\Sigma X$, the viscous evolution part of Eq. (2.1) can be rewritten as

$$\frac{\partial S}{\partial t} = \frac{\partial^2 V}{\partial X^2}. \tag{3.1}$$

The second term in Eq. (2.1), responsible for the planet-disc interaction, is solved individually on the same radial grid. Rewritten in X it is equal to

$$\frac{16}{(GM_*)^{1/2}}\frac{1}{X^3}\frac{\partial}{\partial X}\Lambda S. \tag{3.2}$$

The space derivative in this term is computed using a symmetric two-point finite difference approximation. Then at the end of each timestep the solutions to the first and second part of Eq. (2.1) are combined to yield the surface density across the disc.

In order to solve the time evolution of Eq. (2.1) I need to specify the initial surface density profile of the disc. I do so in a manner similar to Alexander & Armitage (2007), and choose the initial surface density profile to be that of a steady disc

$$\Sigma = \frac{\dot{M}_0}{3\pi\nu}\left(1 - \sqrt{\frac{R_{\rm in}}{R}}\right)\exp\left[-\frac{R}{R_{\rm d}}\right]. \tag{3.3}$$

In the above equation $\dot{M}_0$ is the initial disc accretion rate, $R_{\rm in}$ is the location of the inner disc edge and $R_{\rm d}$ is the location of the outer disc edge. The term in brackets is present due

to the inner boundary condition where the surface density is put equal to zero, to allow for matter to be accreted onto the star, and the exponential term is related to the size of the disc and takes care of the exponential cut-off beyond the outer disc edge. I use an open boundary condition for the surface density at the outer disc edge.

I adopt a disc lifetime of 3 Myr, similar to Bitsch et al. (2018). The initial mass accretion rate was set to be $\dot{M}_0 = 10^{-7}\,\mathrm{M_\odot yr^{-1}}$, in accordance with observations of young protoplanetary discs by Manara (2014). The evolution of the mass accretion rate is set by the viscosity parameter α and the initial size of the disc. If I adopt a viscosity parameter of $\alpha = 0.0054$, which is the value used in Bitsch et al. (2015b), an inner disc edge at 0.1 au and an outer disc edge at 70 au, the mass accretion drops to around $\dot{M} = 10^{-8}\,\mathrm{M_\odot yr^{-1}}$ in 3 Myr. This is in accordance with the model suggested by Hartmann (2009) (black line on right plot in Figure 1.1). However, note that in some models I use a reduced α in the mid-plane of the disc. The reduced α is set to be 10^{-4}, in accordance with Pinte et al. (2016), and results in gas accretion rates of order $1\,\mathrm{M_J/yr}$ (see section 4.6). For the boundary conditions at the disc edges, I simply put the viscous radial velocity to be zero. Further, I let the disc itself stretch several times beyond R_d by increasing the width of the grid-cells on the X-grid by a factor of 2.5. The grid I use has a total of 5000 grid points.

I calculate the time-step dt for the simulations as the global minimum of

$$\mathrm{d}t = \frac{(\Delta R)^2}{\nu}, \tag{3.4}$$

where ΔR is the grid spacing in the semimajor axis. For the standard set of parameters presented in this chapter that results in a timestep of a few years. However, preliminary simulations showed that a timestep this big results in unstable solutions, and therefore I use a timestep that it ten times smaller instead. Since I do not model the formation of the planetary core, but start the planets at pebble isolation mass, I need to consider the time it takes to reach this stage. Johansen & Lambrechts (2017) measure the time it takes for a planetesimal to grow up to $0.1\,\mathrm{M_\oplus}$ via pebble accretion, and the result varies a lot depending on the semimajor axis. For a planet initiated at 15 au it takes between $1 - 2$ Myr. To reach pebble isolation mass, which is around $20\,\mathrm{M_\oplus}$ at 15 au in a disc with low viscosity and and increasing with semimajor axis, one would have to add some time to this. Due to this uncertainty in the growth time-scale of the planetary core, I perform four simulations for each planet, where they are inserted after 2.0, 2.2, 2.4 and 2.6 Myr of disc evolution. Furthermore, it takes some time for the disc and planet to reach equilibrium after the planet has been inserted into the disc. Therefore, if a planet is supposed to be introduced in the disc after 2.0 Myr of disc evolution, I actually insert it a while before this and let it reach equilibrium with the disc before gas accretion and migration is initiated. The time to reach equilibrium depends on the mass and location of the planet, and is varied between simulations.

I only consider a central star of one solar mass in my simulations. The part of the protoplanetary disc that is closest to the star is assumed to be truncated by the star's magnetic field. I do not take this effect into account; therefore, I will neglect the part of the disc interior of 1 au. When a planet migrates interior of 1 au, I simply end the

simulation. Furthermore, I will introduce a surface density floor to the simulation, so that if the planet opens up a gap that is deeper than 10^{-4} times the unperturbed surface density, I set the surface density at that point in the disc to be equal to this floor value. The unperturbed density is calculated using linear interpolation between one point at each side of the gap. Since there might be some material piling up close to the gap edges, I use points several scale heights away from the planets location, where the exact number of scale heights are varied between the simulations. As mentioned in section 2.1.1 of this thesis, linear interpolation is also used to find the values (p_1,...,p_8) used in Eq. (2.11). To do so I first calculate the unperturbed β using linear interpolation. Then I use this together with the temperature gradient ξ, which is constant throughout the simulation, to interpolate between the values found in Table 1 from D'Angelo & Lubow (2010).

Chapter 4

Results of the simulations

In this chapter I will begin with presenting results from the most basic model, that of an unperturbed disc (section 4.1). Then in the sections following that I will add more details to the model. The first step is to add a planet and model the resulting planetary gap (section 4.2). In this section I will compare the gap depths obtained in my own simulations with those of others. Now in my simulations I wish to initiate the planet at its pebble isolation mass, so the next step is to calculate the pebble isolation mass in my code (section 4.3). Once this is done, I will add planetary migration (section 4.4). I will start with a very simple model of only Type-I migration, then I will add Type-II migration. Since it is disputed whether or not Type-II migration actually exist, I will also construct a model to mimic the scenario when the migration is governed entirely by the disc torques which are reduced due to the opening of the planetary gap. In my last most complete migration model I will model migration in a self-consistent manner using the same torque density as I use to model the planetary gap. So up to this point I have modeled a planet of constant mass that migrates in an evolving disc. The final step will be to include the accretion of gas onto the planetary core (section 4.5). I will use two different prescriptions for the gas accretion rates and begin with comparing them to each other. Then I am going to combine these two models of gas accretion with the different models for planetary migration (section 4.6-4.8). At this stage I will have a planet that both migrates and grows. For each of these models I will look at the resulting growth tracks, discuss how realistic they are and compare them to observations. At the end of the chapter I will make a summary of the results (section 4.9).

4.1 The unperturbed disc

In this first most basic model I model the evolution of an unperturbed disc, that is a disc with no planet in it. The evolution of the unperturbed surface density and unperturbed disc accretion rate is shown in the top panels of Figure 4.1 as a function of semimajor axis. In the bottom panel I plot the evolution of the disc accretion rate in the innermost part of the disc. During 3 Myr the disc accretion rate decreases from $10^{-7}\,\mathrm{M_\odot yr^{-1}}$ to $10^{-8}\,\mathrm{M_\odot yr^{-1}}$,

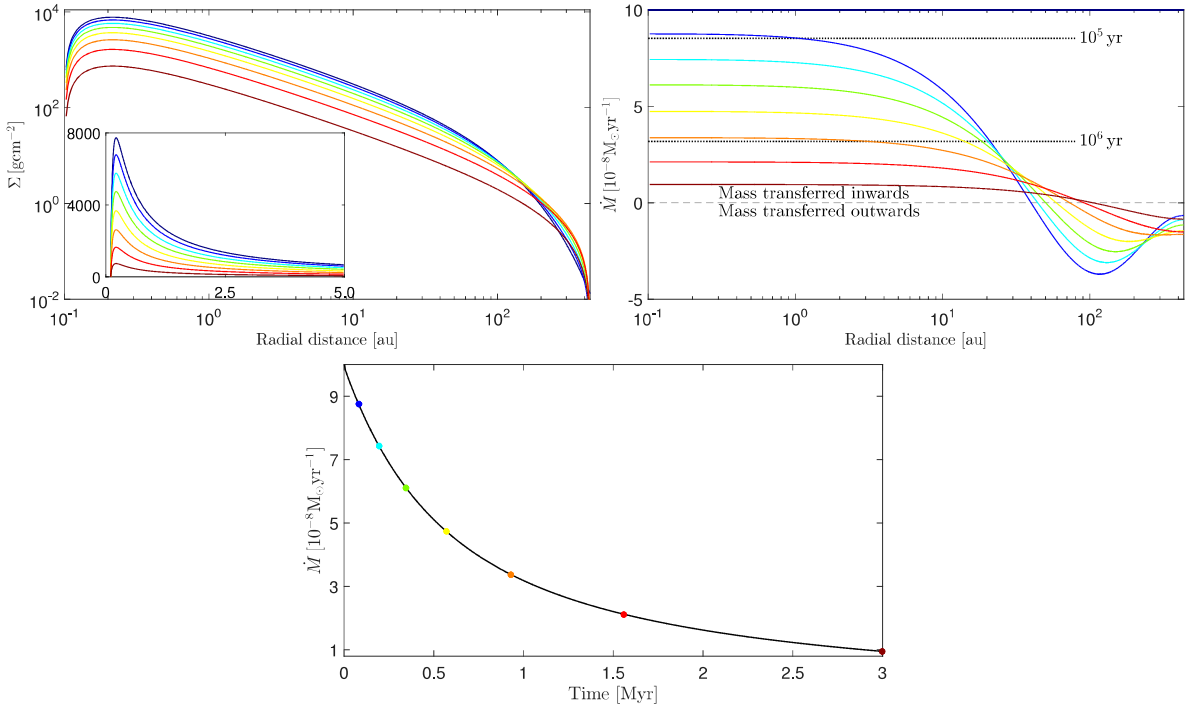

Figure 4.1: Left: Time evolution of the unperturbed surface density versus semimajor axis for a viscous accretion disc with viscosity parameter $\alpha = 0.0054$, inner disc edge $R_{\rm in} = 0.1\,{\rm au}$, outer disc edge $R_{\rm d} = 70\,{\rm au}$ and a lifetime of $3\,{\rm Myr}$. The small plot is a zoomed in version of the big plot with non logarithmic axis. Right: Time evolution of the unperturbed disc accretion rate versus semimajor axis. Dotted lines has been added to the plot to mark 10^5 and 10^6 years of evolution. Bottom: time evolution of the disc accretion rate in the innermost part of the disc. The decrease is following the model of Hartmann (2009), see black line on right panel of Figure 1.1. The dots mark the times when the lines in the top panels were drawn.

which is in accordance with the model suggested by Hartmann (2009) (black line on right plot of Figure 1.1). As can be seen in the plot, the decrease in disc accretion rate is non-linear. Hartmann et al. (1998) expressed this decrease as $\dot{M} \propto t^{-\eta}$ with $1.5 \leq \eta \leq 2.8$.

The negative mass accretion rate seen in the outer part of the disc is present because, as discussed in the introduction, in order for mass to be accreted onto the star angular momentum must be transported outwards in the disc. The outward mass transfer also causes the surface density to increase in the outer parts of the disc. The region of outward mass transfer moves further away from the star with time, as can be seen in the right plot.

4.2 Planetary gaps

In the previous section I modeled how the disc evolved when there was no planet in it. In this section I will add a planet to the disc. So what will happen when I do so? The planet will excite density waves in the disc which carry angular momentum away from the planet and deposit it in the disc via viscous dampening. This angular momentum deposition leads to the opening of a planetary gap; however, instead of directly modeling the interaction between the planet and the disc I choose to instead apply a 1-D torque radially across the disc. Further I assume that the density waves are damped instantaneously. This result in narrower gaps, and might be a bad approximation since we know from observation of mm sized dust that the gaps in protoplanetary discs are quite wide. However, for simplicity, and since it is not certain how well the dust is coupled to the gas, I will use this approximation regardless.

The resulting planetary gaps can be viewed in the upper left panel of Figure 4.2. In this figure we see that high-mass planets open up deeper and wider gaps than low-mass planets. The exact depth of the gap is very dependent on the shape of the torque profile (see e.g. Hallam & Paardekooper 2017), and varies a lot depending on which model is being used, as can be seen in the lower panel of Figure 4.2. The difference between the models increases with increasing planetary mass, especially the gaps formed in my 1-D simulations become very deep for massive planets. It is well known that 1-D models produce narrower and deeper gaps than their higher dimensional analogs (e.g. Lin & Papaloizou 1986b; Kanagawa et al. 2015). Hallam & Paardekooper (2017) performed an extensive analysis of the difference between 1-D and 2-D models and found that the difference still remains even if they apply the same torque density distribution radially across a 2-D model. They suggest that the difference originates from the fact that 2-D/3-D simulations are influenced by instabilities which results in an unstable gap-edge, instabilities which are not present in 1-D simulations. Two such important instabilities are the *Rayleigh instability* and the *Rossby wave instability*.

The Rayleigh instability sets in if the criterion for stability of a rotating disc $d(R^2\Omega)/dR \geq 0$, is violated (Chandrasekhar, 1961). What this means is that the specific angular momentum must increase outwards. If this condition is violated the system will be able to reach a lower energy state by radially mixing material, and so the system becomes unstable. The stability condition can be violated due to a deviation from Keplerian rotation speed of

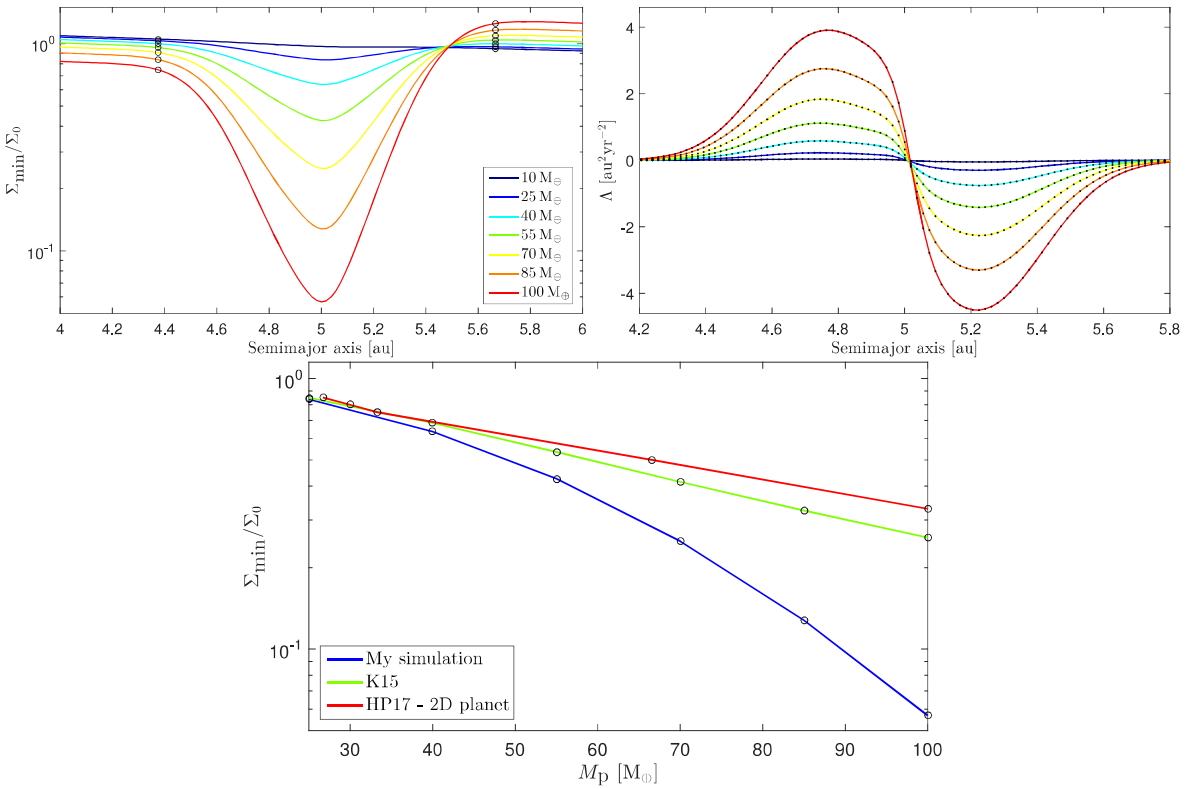

Figure 4.2: Left: Gap-profiles created by the torque density distributions showed in the left panel. Right: Torque density distributions for planets of different masses located at 5 au in a disc where $\alpha = 0.004$ and $H/R = 0.05$ (Eq. (2.10)). Bottom: Gap depths as a function of planetary mass for different models. The gap depths obtained from my own simulations are the same as in the upper left panel, they are calculated using linear interpolation between the points marked with circles on the upper left panel. The curve labeled "K15" is obtained using Eq. (2.24) from Kanagawa et al. (2015), this empirical formula has been obtained from 2-D hydrodynamical simulations. The curve labeled "HP17 - 2D planet" is from a 2-D hydrodynamical simulation by Hallam & Paardekooper (2017).

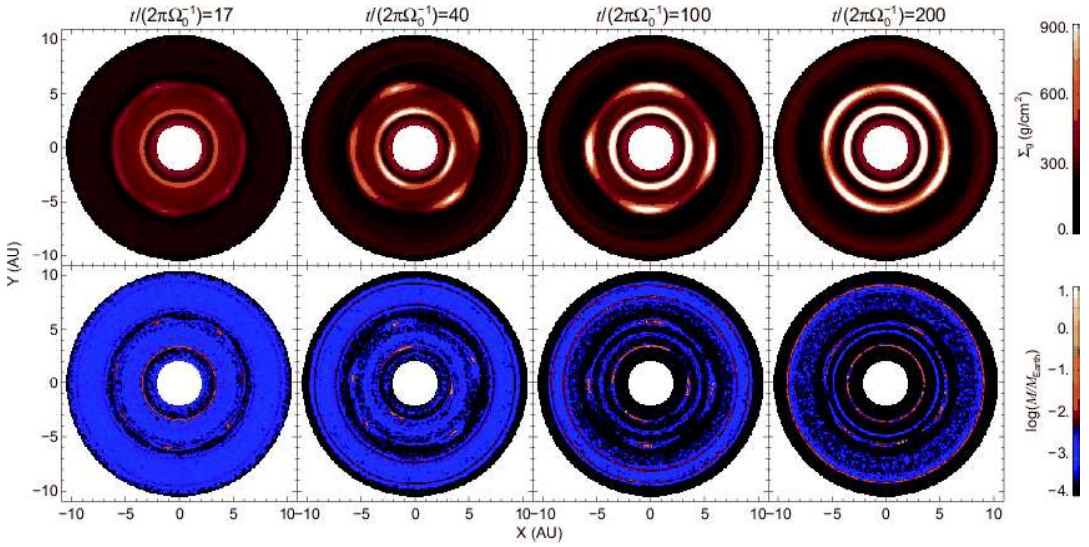

Figure 4.3: Figure adapted from Lyra et al. (2008). Snapshots of a disc of gas (top panel) and a disc of solids (bottom panel) taken after the number of orbital periods indicated above the panels. The vortices triggered by the Rossby wave instability result in trapping of solid particles and gas. This occurs already after 17 orbital periods, which is the time indicated above the leftmost panels.

disc material close to the planet. The approximation of Keplerian velocity is never fully accurate due to the radial pressure gradient in the disc that causes the gas to rotate at a sub-Keplerian speed. This deviation is further increased if a steep surface density gradient is present. The deviation from Keplerian rotation affects the angular momentum transfer at the gap and can, if large enough, violate the Rayleigh criterion. When this occurs the angular momentum transfer becomes enhanced, which results in a shallower surface density gradient and thus a shallower gap depth. The Rossby wave instability, which occurs due to the formation of Rossby vortices by the shear in velocity of disc material close to the planet, is only present for steep density gradients and results in the formation of a turbulent gap edge (see Lovelace et al. 1999; Lyra et al. 2008). This promotes angular momentum transfer, which decreases the density gradient and results in a shallower gap, similar to above. The formation of vortices by the Rossby wave instability is shown in Figure 4.3.

Hallam & Paardekooper (2017) conclude that they can explain the discrepancy between 1-D and 2-D simulations by the absence of the Rossby wave instability in 1-D simulations. This would also explain why the discrepancy is small for low-mass embedded planets, since only gap-opening planets can violate the Rossby wave instability. The Rossby wave instability is only significant for relatively low viscosities; however, the limit at which it becomes significant varies in the literature. Kanagawa et al. (2015) performed a similar investigation as Hallam & Paardekooper (2017), but instead of the Rossby wave instability they explained the difference by a combination of three processes: 1) the deviation from

Keplerian angular velocity due to the pressure gradient, 2) the violation of the Rayleigh stable criterion due to high density gradients at the gap-edge, and 3) the effect of wave propagation which causes the angular momentum to be deposited in a wider region of the disc. They reported that the first two processes make the gap shallower, while the third makes it both shallower and wider. In their complete model they take all these effects into account and obtain 1-D gaps which are consistent with hydrodynamical simulations.

A combination of the processes above may thus explain why the gaps produced in my 1-D simulations are considerably deeper than the gaps formed in 2-D hydrodynamical simulations. The curve labeled "K15" in the bottom panel of figure 4.2 was calculated using Eq. (2.24). This empirical formula, which has been obtained from 2-D hydrodynamical simulations, results in much shallower gaps than my 1-D simulations, and agrees fairly well with the 2-D hydrodynamical simulations of D'Angelo & Lubow (2010).

The fact that the gaps produced in my simulations are too deep will have multiple effects on the evolution of the system, e.g. a faster transition to the slower Type-II migration, less mass flowing across the gap, and lower pebble isolation masses. The gas accretion rate onto the planet will also be affected. Because of this I will use both gap depths resulting from my own simulation and gap depths calculated using the equation from Kanagawa et al. (2015) to calculate the migration and gas accretion rates in the following sections. From the discussion above I conclude that in order to produce an accurate self-consistent model of gap-formation in one dimension, a more advanced torque density distribution than the one we use is required, using e.g. the angular momentum transport equation of Kanagawa et al. (2015).

4.3 Pebble isolation mass

In this section I am going to calculate the pebble isolation mass using the surface density profile obtained in the previous sections, and compare it to results of 3-D simulations. This I do because I wish to start the planet at its pebble isolation mass in my complete simulations. A planet reaches pebble isolation mass when it can perturb the surface density enough to create a positive radial density gradient that counteracts the negative radial gradients of temperature and scale height. This causes the gas outside the planet to no longer orbit at sub-Keplerian velocities, and results in that the pebbles no longer lose angular momentum due to drag. Once the planet reaches pebble isolation mass, the pebbles will thus start to pile up outside the planetary orbit; hence, hindering further pebble accretion onto the core.

In my simulations the pebble isolation mass is calculated by finding for which planetary mass the radial pressure gradient is zero, an example is shown in the right panel of Figure 4.4. The formula from Bitsch et al. (2018) that was presented in section 2.2, Eq. (2.17), was derived in a similar way from fitting results of 3-D hydrodynamical simulations of planet-disc interactions. As discussed in the previous section, the gaps produced in 1-D simulations are deeper than their higher dimension analogs. The result will be that a lower planetary mass is required to reach pebble isolation in my simulations, compared to

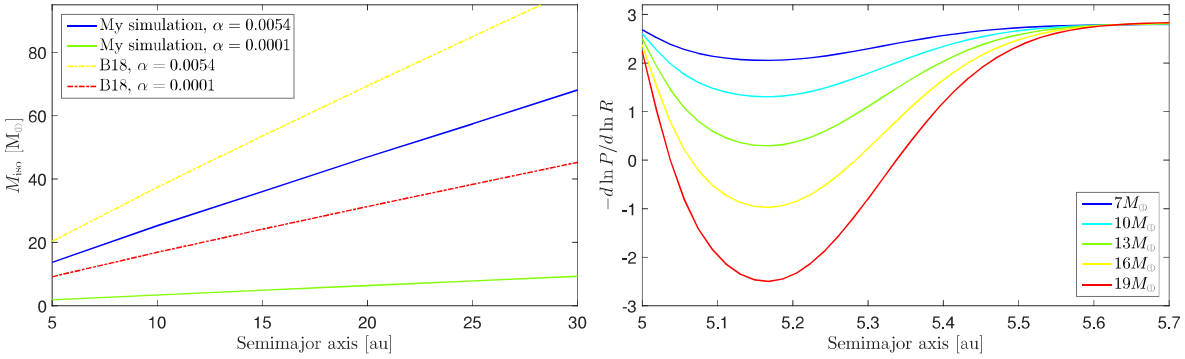

Figure 4.4: Left panel: Pebble isolation masses obtained from my own simulation and from Eq. (2.17) of Bitsch et al. (2018) as a function of semimajor axis. Masses are shown both for the high α used for disc evolution, and for the reduced α in the midplane of the disc. Right panel: The negative radial pressure gradient as a function of semimajor axis for different planetary masses. The pebble isolation mass is obtained by finding for which planetary mass the radial pressure gradient is zero, in this particular case it is for a planet of mass slightly larger than $13M_\oplus$.

the masses obtained from using Eq. (2.17). This can be seen in the top panel of Figure 4.4 where I have done a comparison between the pebble isolation masses obtained from my simulations and the ones obtained from using Eq. (2.17). For the high α model my simulations yield masses which are around 30% lower than the masses obtained using the equation from Bitsch et al. (2018). For the reduced α model this difference increases and my simulations now yield masses which are 80% smaller instead of 30%. This suggests that the gaps formed in my simulations are much more dependent on the viscosity than the ones formed in 3-D hydrodynamical simulations. In all following simulations I will use Eq. (2.17) to calculate the pebble isolation masses, and I will use it together with the reduced α in the mid-plane of the disc.

4.4 Planetary migration

4.4.1 Comparing migration rates

In Figure 4.5 I compare the migration rates obtained from using the different migration prescriptions discussed in Section 2.4. The migration rates of the planets depend on the surface density. The initial surface density profile is proportional to α; however, in this figure I removed this dependency on α so that the initial surface density profile is the same regardless of α. This is to allow for easier comparison.

The Type-I migration prescription from D'Angelo & Lubow (2010) (labeled DL10 in the figure) is proportional to the planetary mass. Since this migration model does not care about the opening of the planetary gap, it results in unreasonably high migration rates for massive planets. In the classical migration picture the planet becomes coupled to the

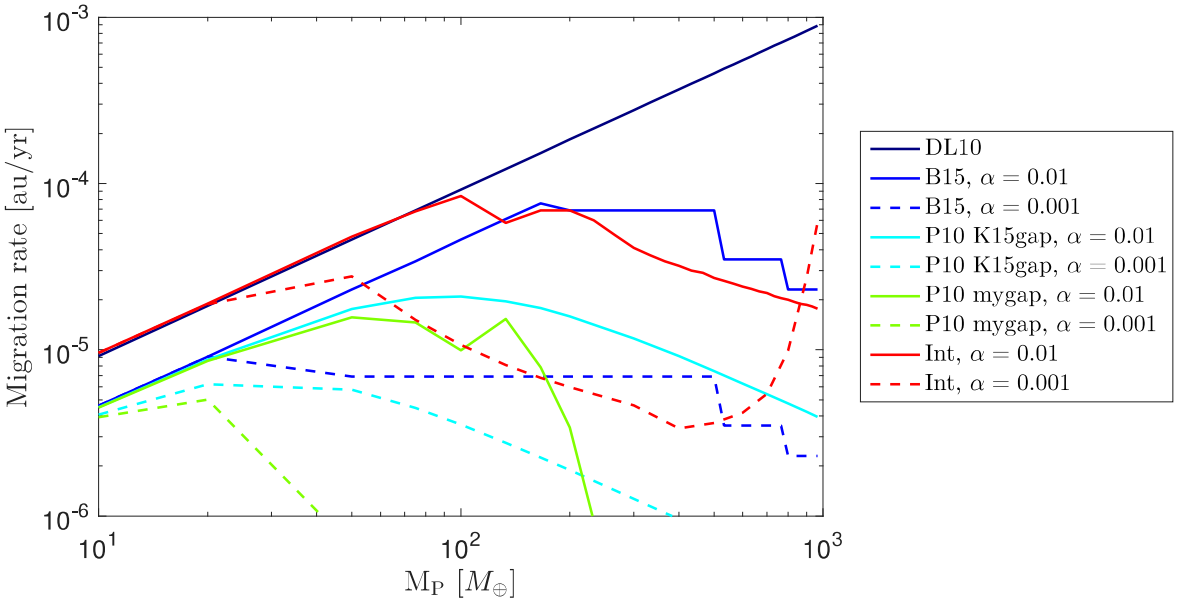

Figure 4.5: Migration rates versus planetary mass for different torque prescriptions and different viscosity models. The curve labeled "DL10" is the Type-I migration rate from D'Angelo & Lubow (2010). The curves labeled "B15" are following the migration prescription of Bitsch et al. (2015b) for Type-I and Type-II migration. The curves labeled "P10" are obtained using the Type-I migration rates from Paardekooper et al. (2010) multiplied by the gap depth, where I use gap depths both from Kanagawa et al. (2015) and from my own simulation. The migration rates labeled "Int" are calculated in a self consistent manner by using the same torque density distribution of D'Angelo & Lubow (2010) as I use to calculate the planetary gaps. For the migration rates where I use my own planetary gaps (curves "P10 mygap" and "Int") I measure the rates at 10^3 yr for $\alpha = 0.01$ and at 10^4 yr for $\alpha = 0.001$.

viscous evolution speed of the disc when a sufficiently deep gap, here taken to be 10% of the unperturbed surface density, is opened up. This results in lower migration rates than for Type-I migration, and migration in this regime is called Type-II migration. For very deep gaps the Type-II migration speed can be even further reduced. In the model labeled B15 I follow the migration prescription of Bitsch et al. (2015b) where they use both Type-I migration and Type-II migration. Unlike Bitsch et al. (2015b) I have not used smooth transitions between the different migration regimes, which is what causes the sharp transitions in migration rates seen in Figure 4.5. This migration model yield migration rates that are more reasonable than the DL10 model for massive planets; however, for $\alpha = 0.01$ a Saturn mass planet at say 10 au would still reach the inner edge of the disc within 10^5 yr. For a lower viscosity the planetary gaps become deeper, which result in a faster transition to Type-II migration and lower migration rates. In this scenario it would take the same planet as above around a millions years to reach the inner disc, which is more reasonable. For very high planetary masses the perturbation on the surface density due to the planet becomes huge in my model, resulting in large torques on the planet. If this is a physical effect or an numerical effect I can not tell, and therefore I will not look deeper into migration in this regime.

Type-II migration could only occur if matter is prevented from crossing the planetary gap, thus dividing the disc into an inner and outer part. Since this migration model often results in that planets migrate all the way to the inner disc, a lot of effort has been put into coming up with an alternative scenario. If as discussed in section 2.4 gas isn't prevented from crossing the planetary gap, there will be no separation between the inner and outer disc and thus the planet will continue to migrate under the actions of the disc torques. Because of the low surface density in the gap region, these torques will be reduced, and thus the migration rates should decrease as well. Kanagawa et al. (2018) perform 2-D hydrodynamical simulations and show that the torque on the planet is decreasing roughly linearly with the gap depth. I mimic this scenario in the model labeled P10, and I do so using the Type-I torque prescription from Paardekooper et al. (2010), where the unperturbed surface density is exchanged for the perturbed one. From the figure it is clear that this migration model indeed results in lower migration rates than in the typical Type-II scenario. Since this model depends on the depth of the planetary gap, and since I know that the gaps produced in my simulations are too deep, I use gap depths both from my own simulations and gap depths obtained using equation 2.24 from Kanagawa et al. (2015). The gap depths from Kanagawa et al. (2015) are shallower than mine for massive planets, which results in higher migration rates than when I use the gaps from my own simulations. When I use gaps from my own simulations the migration halts long before Jupiter masses are reached. For low viscosities the same would be the case for the gaps from Kanagawa et al. (2015).

In the last migration modeled labeled Int I use the same torque density to model migration as I use to model the opening of the planetary gap. This is my most complete and self-consistent model of migration. In this model I do not make a transition to Type-II migration, but let the planet migrate entirely due to the actions of the disc torque. Because of this I would have expected these migration rates to follow the P10 model;

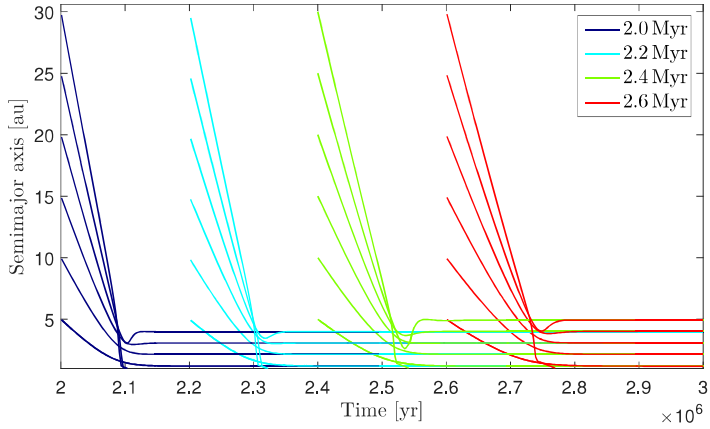

Figure 4.6: In this plot I show the migration tracks for planets of constant mass that start at different semimajor axis and at different times during disc evolution. I have used the migration prescription from Bitsch et al. (2015b) to produce this plot, and since there is no easy way to separate the α used for disc evolution from the one used for migration in this model, I use the same for both ($\alpha = 0.0054$). The mass of the planets in the plot is the pebble isolation mass at their initial locations, calculated using the equation from Bitsch et al. (2018) together with the reduced α in the mid-plane of the disc.

however, looking at the figure I find that the migration rates instead follow the classical Type-I/Type-II migration model. One difference between the models is that the P20 model is directly proportional to the perturbed surface density, while the Int model is proportional to the radial integral of the perturbed surface density. Type-II migration should only exist if much of the gas is hindered from crossing the planetary gap, so it would seem that this might be the case in my 1-D simulations. If so, that would be another difference between 1-D simulations and 2-D simulations, since Dürmann & Kley (2015) used 2-D simulations to show that gas do flow across the gap on horseshoe orbits. I will investigate this further in section 4.8.

4.4.2 Type-I and Type-II migration tracks

In Figure 4.5 I made a comparison between different migration rates, now lets move on to see how the migration tracks of planets might look like. In Figure 4.6 I have plotted the semimajor axis evolution for planets of constant mass using the Type-I and Type-II migration prescription from Bitsch et al. (2015b), this I have done using multiple one-planet simulations. The planets in the plot have different initial locations and are initiated at different times during disc evolution. The mass of the planets are set to be the pebble isolation mass at their respective initial location, calculated using Eq. (2.17) together with the reduced α in the mid-plane of the disc. Since the pebble isolation mass increases with semimajor axis, and the Type-I migration rate is proportional to the planetary mass, the planets that start at 30 au reach the inner part of the disc in approximately the same

amount of time as the planets starting at 5 au.

If a planet migrates past 1 au the simulation is terminated; however, in Figure 4.6 the migration of most planets stop before they reach 1 au. From the figure I can tell that more massive planets stop migrating further out in the disc, up until one reaches masses of around 30 $M_\oplus$, after that the planets continue to migrate all the way to 1 au. The reason for this behavior is the following. The migration rate equals zero only if the total torque on the planet (Eq. (2.29) to (2.33)) equals zero. The only variable in these equations that changes during the simulation is β, the negative slope of the logarithmic surface density. In my simulations I calculate β by taking the derivative between two points taken multiple scale heights away from the planet's location. For the nominal disc parameters that I use, the total torque equals zero only when $\beta \approx 0.54$. For $\beta < 0.54$ the migration changes direction to outwards.

Now Type-I migration is derived for the case when the surface density is largely unperturbed by the presence of the planet, and looking at the unperturbed surface density profile in Figure 4.1, $\beta > 0.54$ at 30 au and should increase towards 1 au. However, when a planet opens up a gap in my simulations it results in some mass piling up outside the planet. One explanation for this could be if some matter is prevented from crossing the planetary gap. If so then the amount of matter that is being piled up increases with gap depth. Since the gap depth increases for smaller semimajor axis, this results in more mass being piled up closer to the star. This effect can be seen multiple scale heights away from the planetary orbit, and because of this β decreases towards the star. Since this effect is larger than the increase of β due to the unperturbed surface density profile, the planets eventually reach a position where $\beta \approx 0.54$. More massive planets open up deeper gaps and thus reach $\beta \approx 0.54$ further out in the disc. If the planets are more massive than around 30 $M_\oplus$ they enter the Type-II regime before this occurs, and continues to migrate all the way to 1 au.

Since this effect is caused by the planet, and Type-I migration is derived for an unperturbed disc, it is most likely not physical. It could be avoided by using a smooth transition between Type-I and Type-II migration, occurring before this effect becomes visible. Another alternative is to change the condition for entering into Type-II migration, essentially making the required gap depth shallower. This is not something I will do in the following simulations. For simplicity, and in order for it to be easy to compare different models between each other, all future simulations will have planets starting at the same locations, masses and times as in Figure 4.6.

4.5 Gas accretion

As the final step I am going to add gas accretion onto the planetary core in my model. I use two different analytical prescriptions for the gas accretion rates (see 2.3). The resulting gas accretion rates are compared in Figure 4.7. The model labeled B15 has two regimes: as long as the envelope mass is less massive than the mass of the core the gas accretion rates increase with planetary mass; when the envelope mass grows larger than the core

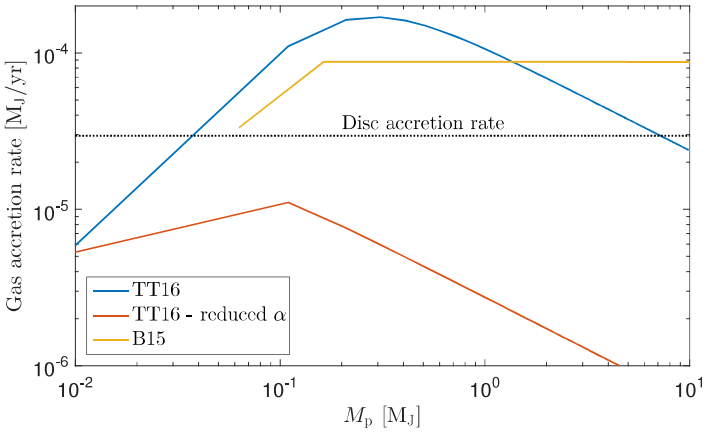

Figure 4.7: Gas accretion rates as a function of planetary mass for the models of Tanigawa & Tanaka (2016) and Bitsch et al. (2015b) (see section 2.3). I use the same disc and planet parameters as in Figure 1 of Tanigawa & Tanaka (2016) to produce this plot ($\alpha = 3 \times 10^{-4}$, $H/a = 0.05$, $f = 1$, $a = 5.2\,\mathrm{au}$), and indeed the blue curve labeled "TT16" follows the curve showed in Tanigawa & Tanaka (2016) exactly. The gas accretion rates from Tanigawa & Tanaka (2016) result in timescales for accretion onto Jupiter mass planets that are as short as $10^4\,\mathrm{yr}$ when my nominal disc accretion α is used. Therefore I will use the reduced α from the mid-plane of the disc to model gas accretion when I use the rates from Tanigawa & Tanaka (2016). The reduced α is set to be 10^{-4}, since that results in gas accretion rates on the order of a few $\mathrm{M_J/yr}$ when the planet reaches one Jupiter mass. The model of Bitsch et al. (2015b) has two regimes. As long as the envelope mass is smaller than a certain critical mass, which is roughly equal to the mass of the core, the gas accretion rates increase with planetary mass. Once the critical envelope mass has been reached, the gas accretion rate saturates and is roughly constant with planetary mass. In my model I use a hard boundary between the two regimes for gas accretion, while in reality the transition should be smoother (see Figure 5 of Machida et al. (2010)). I can not as easily separate the viscosity used in gas accretion from the one used for disc evolution in this model, and therefore I will continue to use $\alpha = 0.0054$.

mass rapid gas accretion initiates. At this stage the gas accretion rates are independent on the planetary mass. The sharp transition between the two regimes comes from fitting a very simple formula to the results of Machida et al. (2010), the actual data that they use for fitting features a smoother transition. The model of Tanigawa & Tanaka (2016) has a dependency on both the planetary mass and the depth of the planetary gap, causing the parabolic-like shape.

For the same level of viscosity, the gas accretion rates of Tanigawa & Tanaka (2016) are a few factors higher than the ones from Bitsch et al. (2015b) for planets with masses between 0.1 and 1 Jupiter masses. However regardless of this discrepancy, both models yield gas accretion rates that are much higher than $1\,M_J/Myr$ when $\alpha = 0.0054$ is used. To form gas giants with a mass comparable to Saturn or Jupiter, it is not desirable to have gas accretion rates higher than a few M_J/Myr. In the model of Tanigawa & Tanaka (2016) lower gas accretion rates onto the planet can be obtained by reducing α in the calculation for the gap depths (Eq. (2.24)). This can be motivated if one assumes that the planet is positioned in the mid-plane of the disc, where the viscosity as discussed in section 2.1 is likely lower than in the top-layer of the disc. From the figure we see that using $\alpha = 10^{-4}$ results in more reasonable gas accretion rates. There is no easy way to separate the viscosity used in gas accretion from the one used for disc evolution in the model of Bitsch et al. (2015b), so therefore I will continue to use $\alpha = 0.0054$ in that model.

Now I have added all the steps to my planet formation model, and in the following sections I will combine the above gas accretion rates with the different models for planetary migration showed in section 4.4.

4.6 Type-I & Type-II migration + gas accretion

In this section I use the classical Type-I and Type-II migration model (model labeled B15 in Figure 4.5) together with gas accretion rates from either Bitsch et al. (2015b) or Tanigawa & Tanaka (2016). For the Tanigawa & Tanaka (2016) model I will use gap depths both from my own simulation, and gap depths calculated using the formula of Kanagawa et al. (2015) together with the reduced α in the midplane of the disc. The viscous α is kept at 0.0054 throughout this work.

The results of these simulations can be seen in Figure 4.8. The most obvious concern with these simulations is that the migration rates are so high that the nearly all planets migrate all the was to the inner disc. The only planets that survive are the ones that start far out in the disc and late during disc evolution. This result was expected since one known issue with both Type-I and Type-II migration is that they are too fast, in the sense that the planets migrate tens of au while they grow and end up close to the star unless the embryo starts far away from the star and late in the life-time of the disc. In the simulations where the planets shift migration direction, the planets open up gaps deep enough for β to become smaller than 0.54 while still remaining in the Type-I regime. As discussed in the previous section this is likely not very physical, and therefore those simulations will be discarded.

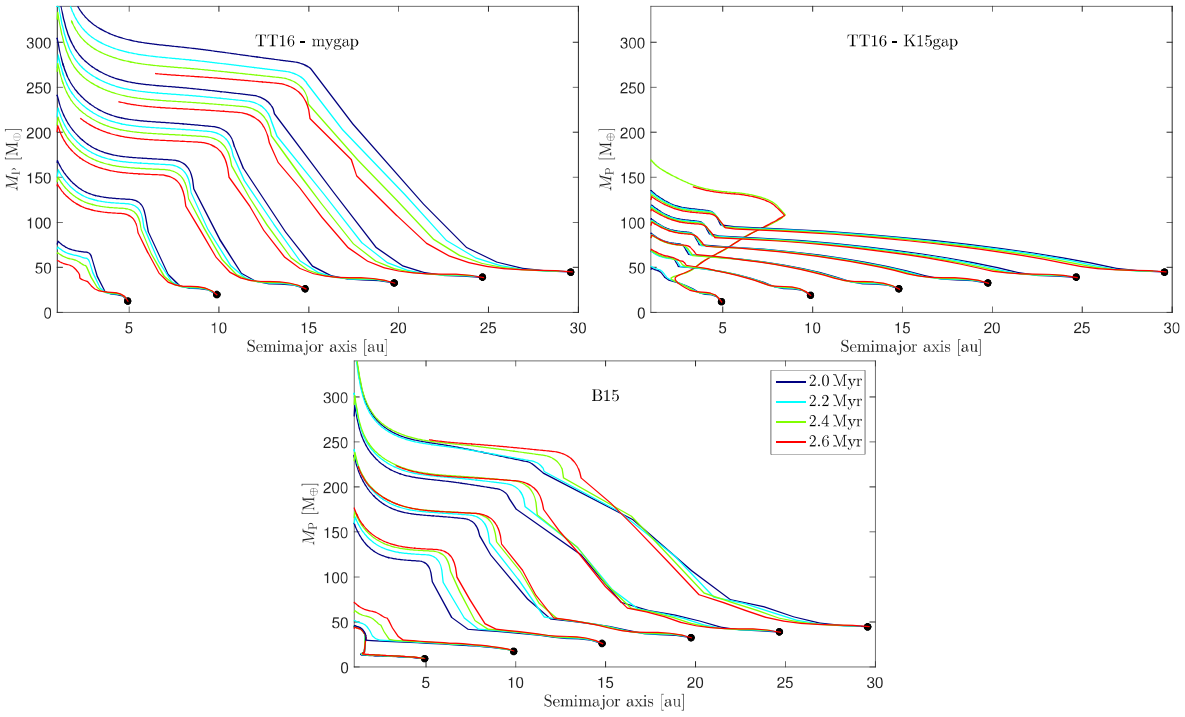

Figure 4.8: Growth tracks of planets resulting from models where I use the migration prescription of Bitsch et al. (2015b), together with gas accretion rates from either Tanigawa & Tanaka (2016) (TT16) or Bitsch et al. (2015b) (B15). The gas accretion rates from TT16 are calculated using either gap depths from my own simulation (mygap) or using the formula from Kanagawa et al. (2015) (K15gap). The black dots mark the pebble isolation mass, and the color of the lines indicate when during disc evolution the migration and gas accretion was initiated. The same coloring scheme will be used in all following plots of growth tracks.

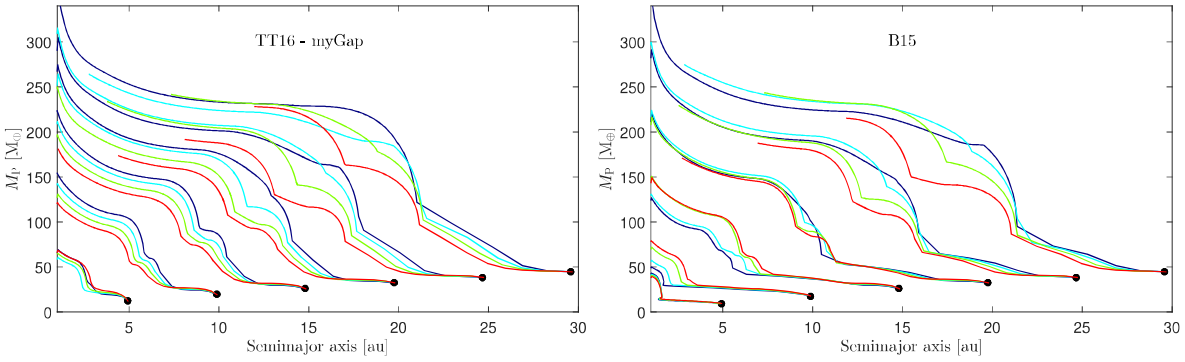

Figure 4.9: These plots are produced using the same simulations as for the B15 and TT16-myGap plots in Figure 4.8, but this time I also take into account the removal of gas from the disc due to gas accretion onto the planet.

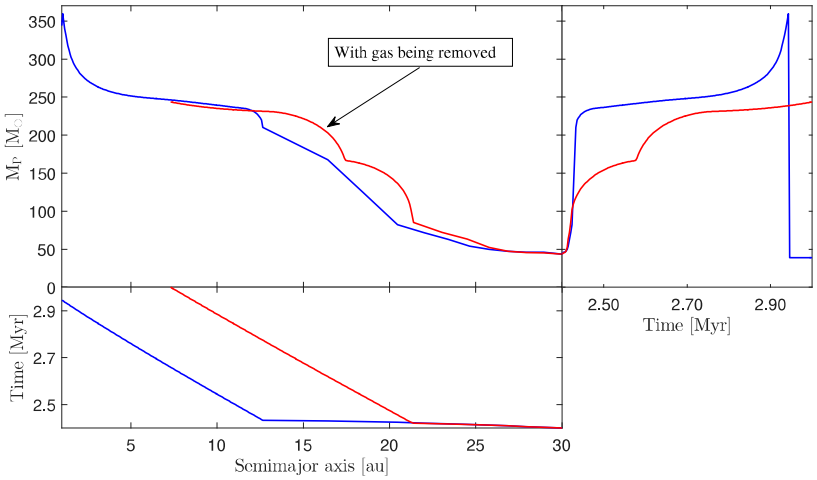

Figure 4.10: These simulations are produced using gas accretion rates from Bitsch et al. (2015b). Blue lines are for simulations where I do not include the removal of gas from the disc, and red lines are for simulations where I do (this coloring will be the same in all plots where I compare between models with and without the removal of gas). Top left panel: growth track for planets starting at 30 au after 2.4 Myr of disc evolution. Right panel: evolution of the planetary mass. Bottom panel: evolution of the semimajor axis.

Regarding the final masses for the planets, the only simulations that do not produce gas giants of Jupiter size are the ones where I use the gap depths from Kanagawa et al. (2015) together with the reduced α. It turns out that for small planetary masses, using the reduced α actually results in deeper gaps than the ones I obtain from my own simulation. This translates into lower gas accretion rates, which means that it will take more time for the planets to carve gaps deep enough to start migrating in the Type-II regime. A longer period of fast Type-I migration means that the planets will come significantly closer to the star before Type-II migration initiates, and reach the inner disc much faster than in the simulations where I use my own gaps or the model of Bitsch et al. (2015b). These planets thus have a much shorter amount of time to accrete gas, and consequently grow less massive.

In Figure 4.9 I redo the same simulations as in Figure 4.8, but this time I also take into account the removal of gas from the disc due to gas accretion onto the protoplanet. I do so by finding the grid cells which are located within one Hill radii away from the protoplanet, and divide the total amount of gas that should be removed equally between these cells. If the resulting effect on the gap depths is so large that the gas accretion rates and migrates rates change significantly, then this back reaction is important and should be taken into account in models of planet formation. After comparing them I conclude that this indeed is the case. Generally the removal of gas from the disc results in lower final masses and shorter migration distances. The final mass is affected more when the gas accretion rates from Tanigawa & Tanaka (2016) are being used, which is expected since these rates are proportional to the depth of the planetary gap.

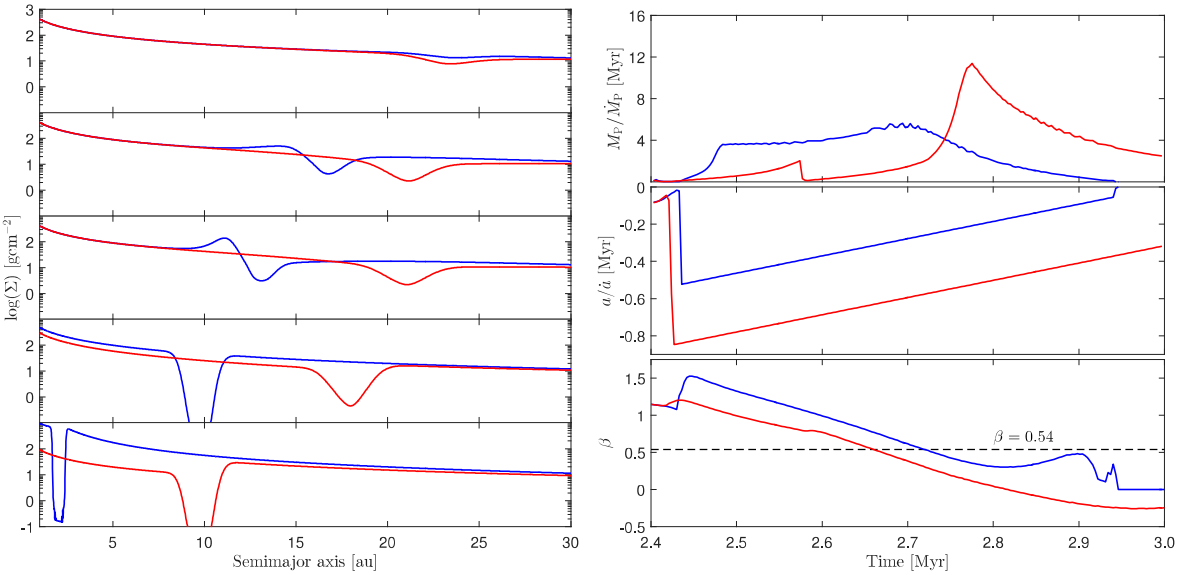

Figure 4.11: These plots are from the same simulations as those in Figure 4.10. Left panel: snapshots of the surface density profile at 5 different moments in time. Top right panel: planetary mass divided by the mass accretion rate. This gives the timescale for gas accretion as a function of time. The non-sharp lines are a numerical effect origin in the low precision used to calculate $\dot{M}_p$. Middle right panel: semimajor axis divided by the migration rate. Similarly this gives the migration timescale as a function of time. Bottom right panel: the unperturbed β as a function of time.

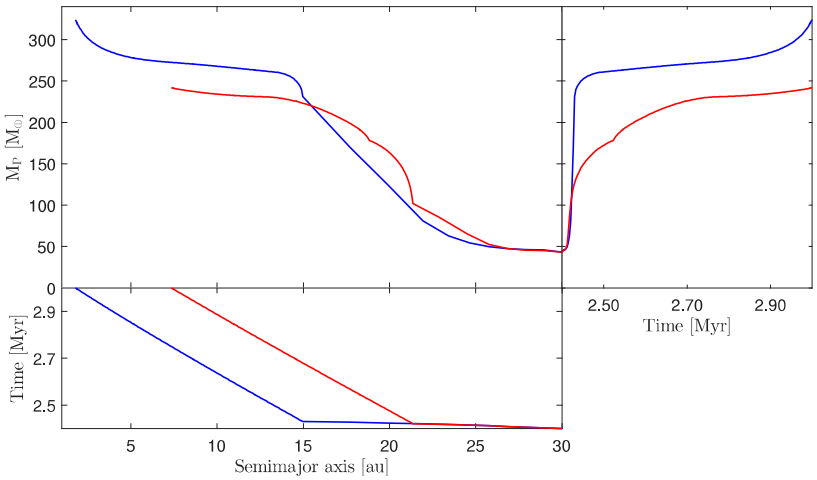

Figure 4.12: These simulations are produced using gas accretion rates from Tanigawa & Tanaka (2016) together with gap depths from my own simulations. Top left panel: growth track for planets starting at 30 au after 2.4 Myr of disc evolution. Right panel: evolution of the planetary mass. Bottom panel: evolution of the semimajor axis.

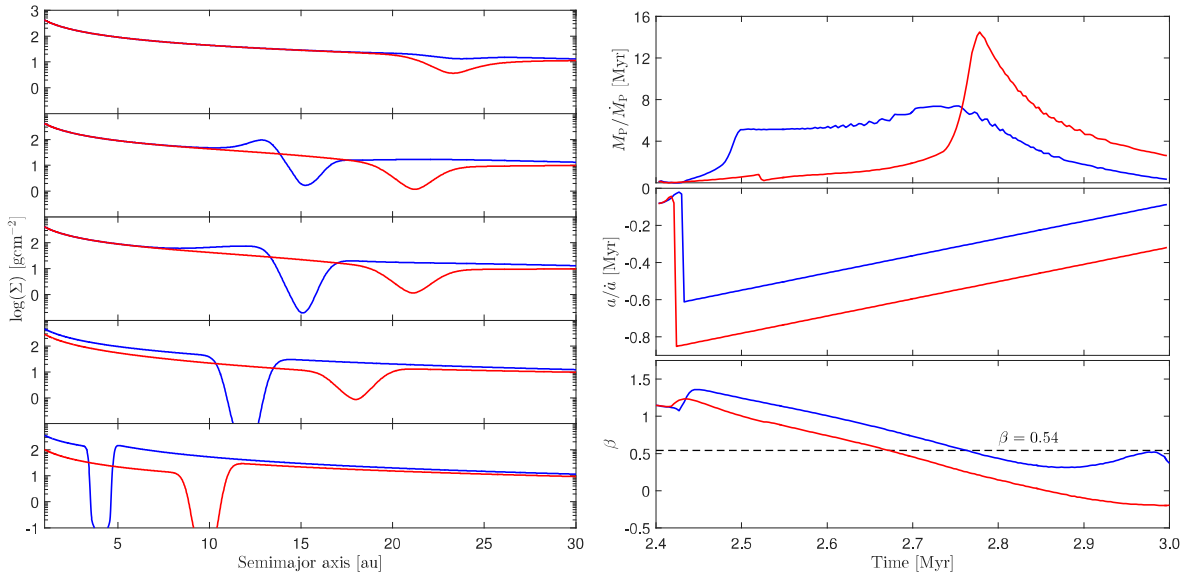

Figure 4.13: These plots are from the same simulations as those in Figure 4.12. Left panel: snapshots of the surface density profile at 5 different moments in time. Top right panel: planetary mass divided by the mass accretion rate. Middle right panel: semimajor axis divided by the migration rate. Bottom right panel: the unperturbed β as a function of time.

I investigate the differences between the models where I include the removal of gas, and the models in which I do not, more thoroughly in Figures 4.10-4.13. In these figures I only look at simulations starting at 30 au after 2.4 Myr of disc evolution. I use gas accretion rates from Bitsch et al. (2015b) in Figures 4.10-4.11, and gas accretion rates from Tanigawa & Tanaka (2016) in Figures 4.12-4.13. In the models where I use gas accretion rates from Tanigawa & Tanaka (2016) I use gap depths from my own simulations. In Figure 4.10 and 4.12 I compare the mass and semimajor axis evolution of the models. In Figure 4.11 and 4.13 I show snapshots of their surface density profiles at 5 different moments in time (left panels), the timescales for gas accretion (top right panels) and migration (middle right panels), and the evolution of the unperturbed β (bottom right panels).

From these figures we learn that the inclusion of gas removal from the disc, at least initially, results in deeper planetary gaps. This leads to an earlier transition to Type-II migration, which is why the migration distance becomes shorter. From the middle right panel of Figure 4.11 and 4.13 we see that the migration timescale also gets longer, which once again is because the transition to Type-II migration happens further out in the disc. Turning to gas accretion, this process is really fast initially when the gaps are shallow and the migration rates are high. The majority of the mass is accreted during the first small time period of Type-I migration. Since the gaps at this point are deeper for the simulations where I include gas, that results in lower accretion rates and once again a shorter period of fast accretion. This is why those planets become less massive, even though the timescale

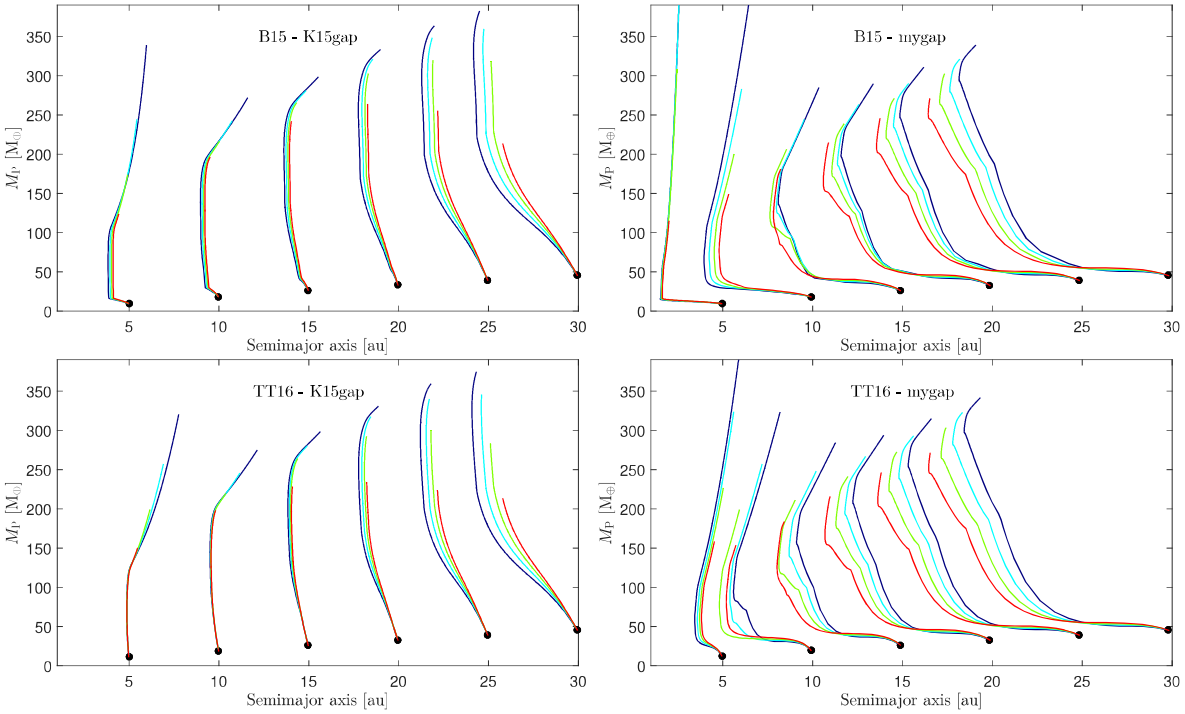

Figure 4.14: In these plots I use the Type-I torque from Paardekooper et al. (2010) together with the perturbed surface density in an attempt to mimic the scenario when Type-II migration does not exist. On each figure I indicate what gas accretion rates that was being used, and which gap depths that are being used for the migration rates (this is the same gap depths used for gas accretion when the TT16 gas accretion rates are being used).

for gas accretion is much shorter for at least half of the evolution (see bottom right panel in Figure 4.11 and 4.13).

Overall the gaps get wider in the simulations where I include the removal of gas. This is expected since I remove gas from the entire Hill radius, which with the current resolution is equivalent to a minimum of 10 grid cells. The pile-up of material interior of the planetary orbit, that is visible in the plots where I do not include the removal of gas, disappears when I do include it. Furthermore, there is a clear dip in the surface density interior to the planet that appears when I include gas removal. This results in that β is lower for the model in which I remove gas from the disc. After around 2.7 Myr of disc evolution β becomes smaller than 0.54, which in the Type-I regime would have resulted in outward migration. However, since Type-II migration is reached much earlier than that, it will not affect the migration.

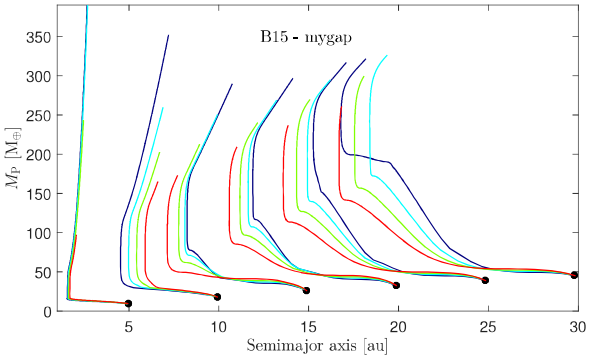

Figure 4.15: This plot is produced using the same simulations that were used to produce the top-right panel of Figure 4.14, the only difference being that I include the removal of gas from the disc due to gas accretion onto the planet in these simulations.

4.7 Type-I $\propto$ gap depth & no Type-II + gas accretion

In the previous set of simulations the migration speed was too fast, resulting in that the planets reached the inner disc in a short amount of time. If there is no Type-II migration, and the torque on the planet decreases roughly linearly with gap depth (Kanagawa et al., 2018), then the migration could potentially be halted before this occurs. I investigate this scenario by using Type-I torques from Paardekooper et al. (2010), which I modify so that they are proportional to the gap depth. For deep gaps this will basically cause the planets to stop migrating, and continue to accrete gas in-situ.

Once again I will use gas accretion rates from both Bitsch et al. (2015b) and Tanigawa & Tanaka (2016). For the migration rates I use both the gap depths resulting from my own simulation and the gap depths from Kanagawa et al. (2015), together with the reduced α. The results of these simulations can be seen in Figure 4.14. Once again the gap depths obtained from using the Kanagawa et al. (2015) formula are deeper for low mass planets, in this case resulting in a shorter period of migration before the planet stops and continue to accrete gas practically in-situ. When the planets grow massive enough β becomes less than 0.54, and the Type-I torque prescription results in outward migration. As mentioned previously this is most likely not physical but a consequence of using this torque prescription in a regime that it was not derived for. However, since the planets at this point migrate so slowly anyway, in most cases it does not make a big difference.

From the results presented above I can conclude that this migration model could solve the problem of too fast planetary migration. The planets that are initiated on a small semimajor axis migrate a very short distance before they stop and continues to accrete gas in-situ, if they migrate at all. The planets that start further out in the disc will migrate further, due to the higher migration rates and shallower planetary gaps. Depending on which gas accretion rates that are being used, and when and where in the disc the planets are initiated, I end up with planets located between $2 - 25\,\mathrm{au}$ and with masses between $100 - 400\,\mathrm{M}_\oplus$.

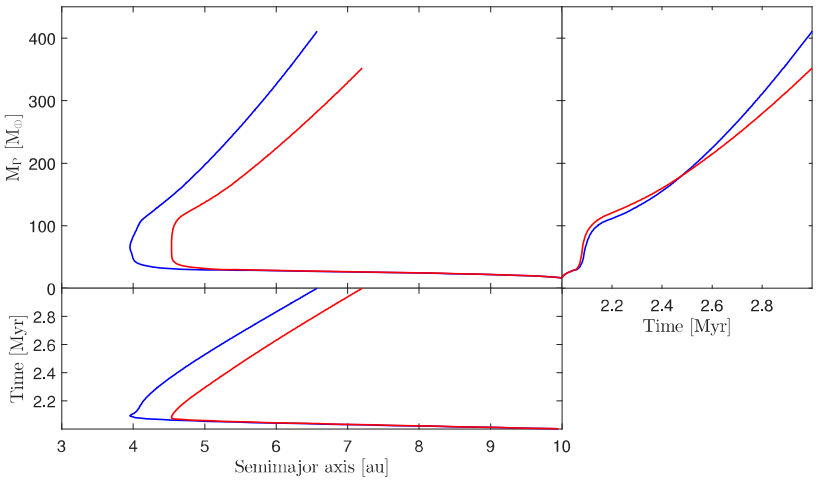

Figure 4.16: These simulations are produced using gas accretion rates from Bitsch et al. (2015b), and migration rates calculated using gap depths from my own simulations. Top left panel: growth track for planets starting at 10 au after 2.0 Myr of disc evolution. Right panel: evolution of the planetary mass. Bottom panel: evolution of the semimajor axis.

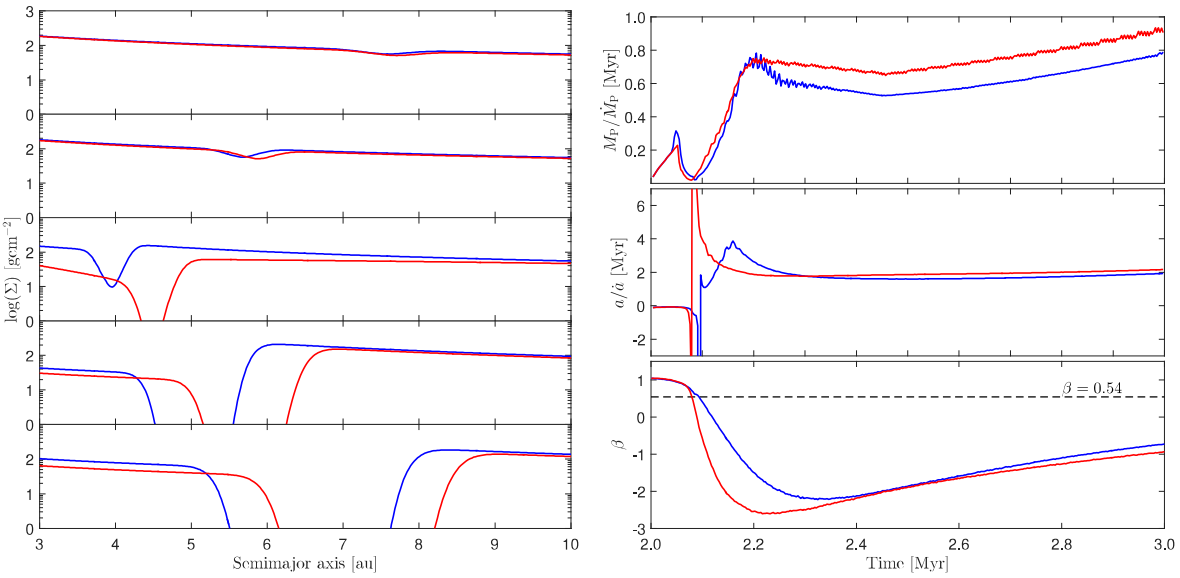

Figure 4.17: These plots are from the same simulations as those in Figure 4.16. Left panel: snapshots of the surface density profile at 5 different moments in time. Top right panel: planetary mass divided by the mass accretion rate. Middle right panel: semimajor axis divided by the migration rate. Bottom right panel: the unperturbed β as a function of time. The simulations in which I include the removal of gas reach $\beta = 0.54$ slightly further out in the disc, and thus reverses its migration direction sooner, but except for that there are no big differences between the simulations.

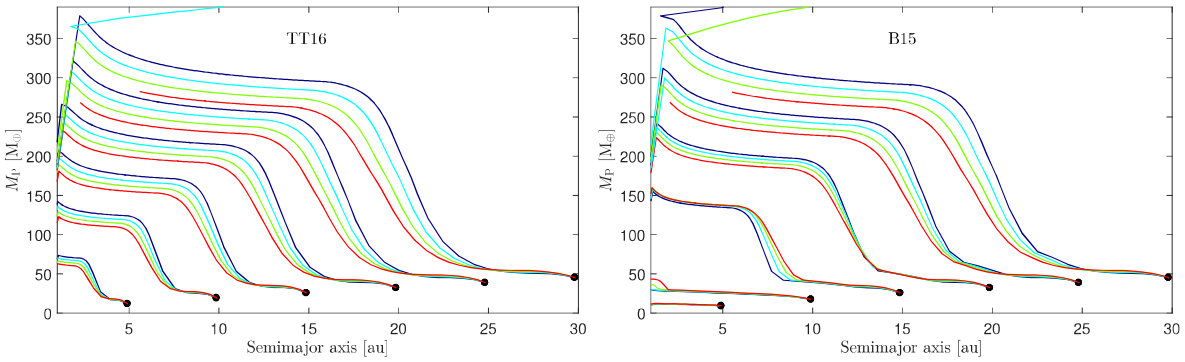

Figure 4.18: In these plots I allow the planet to migrate self-consistently by using the same torque density distribution that I use for the gap-opening. For consistency I then also use the gap depths produced in my own simulation when I calculate the gas accretion rates of TT16.

In Figure 4.15 I perform the same simulations as in the top right panel of Figure 4.14, but now I include the removal of gas from the disc. The effects on planet formation due to this is quite small this time. The planets become a bit less massive and reverse their migration direction sooner, but the final semimajor axis does not change much in most cases. In the previous section the difference in semimajor axis was mostly due to the fact that Type-II migration was reached earlier. Since there is no Type-II migration in this model, the difference in semimajor axis evolution should thus be smaller. Any difference in β would also be less prominent since I multiply by the gap depth, which becomes very deep in my 1D simulations.

In Figure 4.16 and 4.17 I compare the evolution of planets starting at 10 au after 2.0 Myr of disc evolution, for models with and without the removal of gas. The model in which I remove gas from the disc migrates a bit slower due to the deeper planetary gap. The deeper gap also results in that $\beta = 0.54$ is reached further out in the disc. The difference between the timescales for migration and gas accretion is fairly small. Further, the difference between the width of the gaps are less prominent this time. Generally I conclude that, removing the same amount of gas from the disc that is accreted onto the planet, matters less when this migration model is being used.

4.8 Self-consistent planetary migration + gas accretion

In this final set of simulations I let the planets migrate self-consistently using the same torque density distribution that is used to open up the planetary gaps, this is my most complete model. The migration rate of the planet is now proportional to the radial integral of the prescribed torque density times the perturbed surface density. I do not make a transition to Type-II migration in this model. I use the same models for gas accretion as

previously, but now in order to be consistent I only use the gap depths resulting from my own simulations when I use the gas accretion rates of Tanigawa & Tanaka (2016), and not the gap depths from Kanagawa et al. (2015). The results of these simulations can be seen in Figure 4.18.

From Figure 4.5 I expect these growth tracks to look very similar to the analogous ones in Figure 4.8, and indeed this is the case. The growth tracks differ a bit from the ones in Figure 4.8 close to the star, which is because the perturbation on the disc for massive planets close to the inner edge becomes extremely big. The surface density just inside and outside the planetary gap grows very high, resulting in very large torques. Most often the outer torque grows very much larger, causing the planet to migrate so fast to the inner edge that my sampling timestep is too small to catch it. At rare occasions the inner torque wins instead, which causes the planet to make a similar leap in semimajor axis outwards in the disc.

So how comes that these growth tracks resemble the ones where I use Type-II migration? In section 4.4 I argued that this should be the case only if mass is hindered from crossing the planetary gap. This would not have an effect on the model where the migration rate is directly proportional to the perturbed surface density, but would have an effect in this model where the migration rates are proportional to the radial integral of the perturbed surface density. To investigate what happens in this case I picked a typical simulation and plotted the surface density profile and the disc accretion rate at a time when the planet and the disc has reached equilibrium (see Figure 4.19).

From this plot I learn that gas is effectively prevented from crossing the planetary gap. This means that there is no refilling of gas into the inner disc, and so for example if the planet migrates slower than the disc accretes onto the central star, the surface density interior to the planet should be depleted. However, looking at the top panel there is no such depletion visible. The surface density looks unperturbed both interior and exterior to the planetary gap. This all suggests that both the inner disc, the planet, and the outer disc moves with the same radial velocity. So in my 1-D model I end up with classical Type-II migration. Since Dürmann & Kley (2015) used 2-D simulations to show that gas does flow across the planetary gap, and I have shown in my 1-D simulations that gas is hindered from crossing the gap, it would seem that this is yet another discrepancy between 1-D and 2-D simulations.

In Figure 4.20 I performed the same simulations as in the right panel of Figure 4.18, but this time I also take into account the removal of gas from the disc due to mass accretion onto the planet. As can be seen in the plots, this results in lower planetary masses. Since the planetary masses are lower when the inner edge is reached, there are no occasional outward jumps in semimajor axis. Regardless if I remove mass from the disc or not, the fact remains that the migration speed is too fast. Since I use the unperturbed surface density to calculate β in the torque density distribution this was expected. In order to slow down migration enough to prevent the planets from reaching the inner disc, the torque reduction due to the gap must be taken into account.

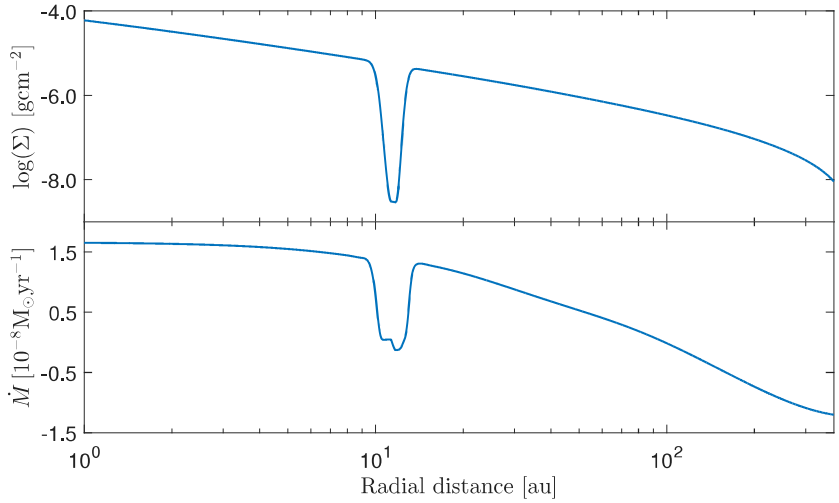

Figure 4.19: Snapshot of the surface density profile (top panel) and the disc accretion rate across the disc (bottom panel) taken at a time when the disc and planet has reached equilibrium. The planet in this specific simulation was initiated at 25 au after 2 Myr of disc evolution. In this simulation I used gas accretion rates from Bitsch et al. (2015b). From the bottom panel we learn that gas is prevented from crossing the planetary gap. Looking at the top panel, gas has neither been depleted or piled-up close to the planetary orbit. This suggests that the planet and the disc moves together with the same speed. So in my 1-D model I end up with classical Type-II migration rates.

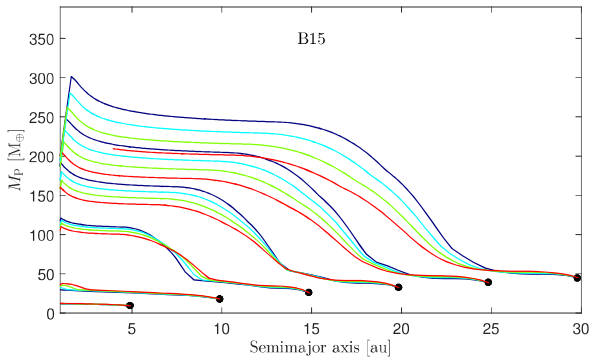

Figure 4.20: This plot is produced using the same simulations as in the right panel of Figure 4.18, but for this plot I also take into account the removal of gas from the disc due to gas accretion onto the planet.

4.9 Summary of results

In section 4.2 I confirmed what was previously known, that 1-D simulations produce deeper gaps than their higher dimensional counterparts. In section 4.3 I see that this results in lower pebble isolation masses than those obtained in higher dimensional simulations. In section 4.5 I compare different models for planetary migration and find that all models, except for the one where the migration rates are directly proportional to the gap depth throughout the simulation, result in migration rates that are so high that the planets are lost to the star. I also find that if I use the same torque density distribution to model migration as I use to model the planetary gaps, I obtain migration rates which are very similar to the classical model of Type-I and Type-II migration. One suggestion to why this might be the case, is that mass is hindered from crossing the gap in 1-D simulations. The simulations show that this indeed is the case for part of the evolution, but not always. Further analyzes are required to fully understand why this is the case.

In order to obtain reasonable gas accretion rates, a lower viscosity in the mid-plane of the disc is required. In section 4.6 I find that $\alpha = 10^{-4}$ yields gas accretion rates on the order of $10^{-6} - 10^{-5}\,\mathrm{M_J/yr}$. The reduced α is further used to calculate the pebble isolation masses. Since the gas accretion rates in one of the two models that I use are proportional to the gap depths, and I know that my gap depths are to deep, I perform additional simulations using gap depths that are calculated from the empirical formula of Kanagawa et al. (2015). The reduced α in the mid-plane of the disc is used to calculate these gap depths. For large planetary masses, this results in much shallower planetary gaps. However, it turns out that for small planetary masses, the gap depths from Kanagawa et al. (2015) are deeper than those produced in my simulations. This affects the simulations where I use the classical Type-I/Type-II migration model. Since the gap depths are deeper for small planetary masses, the gas accretion rates will also be lower, and this results in a longer period of Type-I migration. Because of this, the planets will reach the inner disc edge before they have grown to Jupiter sizes (see Figure 4.8).

In the model where the migration rates arise from the Type-I torque multiplied by the gap depth, the planets migrate a short distance before they stop and continue to accrete gas practically in-situ. In this model the planets migrate a shorter distance when the gap depths from Kanagawa et al. (2015) are used. Regardless of which gap depths that are used, this is the only model in which I am able to form Jupiter like planets that does not have a $40 - 50\,\mathrm{M_\oplus}$ core. Finally I also investigate the effect of gas accretion on the protoplanetary disc. The gas that is accreted onto the protoplanet originates from the disc, and in some simulations I remove the same amount of gas that is accreted onto the planet from the disc. This results in deeper and wider planetary gaps, which leads to longer timescales for gas accretion. The effect on planet migration is most prominent in the model where I make a transition to Type-II migration, and results in shorter migration distances.

Chapter 5

Discussion and conclusions

In this thesis I have performed 1-D simulations of a viscous evolution disc that is perturbed by a protoplanet which migrates and accretes gas. I have considered three different models for planetary migration: in the first model I use standard Type-I and Type-II migration rates; in the second I mimic the case when Type-II migration does not exist and the Type-I migration rates are reduced due to gap-opening; in the third I let the planet migrate self-consistently using the same torque as I use for gap-opening. I use two different models for gas accretion, where one of them takes into account the reduced α in the mid-plane of the disc. The aim has been to investigate what effect planet formation has on disc evolution, the most obvious one being the planet induced gap.

The torque which I apply to the disc in order to produce the planetary gaps assumes instantaneous wave dampening, and does not take into account that there are instabilities occurring in 2-D/3-D simulations which are not present in 1-D simulations. As other authors have concluded previously (e.g. Hallam & Paardekooper 2017; Kanagawa et al. 2015), this results in that the gaps produced in 1-D simulations are deeper and thinner than those produced in 2-D/3-D simulations. I measure the gap depths produced in my simulations, compare them to results presented in other papers and reach the same conclusion. Deeper gap depths translate to lower pebble isolation masses, and further affect the mass at which the transition between Type-I and Type-II migration occurs. It also affects the gas accretion rates in models which depend on the surface density at the location of the planet. The depth of the planetary gaps thus have a big impact on the planet formation process, and correct gap depths could greatly improve models of planet formation.

In order to obtain reasonable gap-shapes in 1-D simulations one needs to use torque prescriptions that take all the effects mentioned in section 4.2 into account. These torque prescriptions can become quite complicated, and therefore authors such as e.g. Kanagawa et al. (2015) have used hydrodynamical simulations to derive empirical fitting formulas for the depths of planetary gaps. Unless a more advanced torque model is being used, one can choose to use these fitting formulas in order to obtain more realistic gas- and migration rates. However, if one wants to learn about the shapes of planetary gaps in order to compare with observations of rings in protoplanetary discs, knowing only the gap depth is not enough. One method to mimic the effect of the Rossby wave instability and

the Rayleigh instability could be to increase the viscosity at the edges of the gap. This would increase the angular momentum transfer at the gap edges and most likely results in a shallower gap. This is something that I will continue to work on.

The gas that is accreted onto the protoplanet is taken from the disc. This implies that when I model gas accretion onto the planet I should also remove the same amount of gas from the disc. Depending on how massive the disc is compared to the planet, and the timescales for mass and migration, this may or may not be important to incorporate into the model. From running simulations with and without the removal of gas, I conclude that it makes a significant difference in most cases. Including it results in deeper and wider planetary gaps, which leads to lower planetary masses. In the case when Type-II migration is included in the model, the transition to Type-II migration occurs earlier, which leads to shorter migration distances. In the case when I only use Type-I migration multiplied by the gap depth, the direction of migration is reversed further out in the disc. Comparison between these two cases shows that it is more important to include the removal of gas when the planet is migrating, than when it is accreting gas practically in-situ.

In my simulations the classical model of Type-I and Type-II migration results in migration rates that are too high. When I use the same torque to model migration as I use to model the planetary gaps, I end up with migration rates that are very similar to the Type-I and Type-II migration rates, even though I do not make a transition to Type-II migration. Type-II migration occurs if the planet stops gas from drifting across the gap, so that the disc is split into two parts. After analyzing my simulations I find out that this indeed is what happens, so in my 1-D model I end up with classical Type-II migration. However, in 2-D simulations mass is supposed to be able to cross the gap even for deep gaps (Dürmann & Kley, 2015), so this seems to be yet another difference between 1-D and 2-D simulations.

The model in which the migration rates arise from the Type-I torque multiplied by the gap depth is the only model in which the planets do not migrate all the way to the inner disc. In these simulations the planet migrates a short distance, after which it continues to accrete gas practically in-situ. In this model I am able to form Jupiter-like planets with core masses of around $10 - 20\,\mathrm{M}_{\oplus}$. This model is supported by Kanagawa et al. (2018) where they show that the torque on the planet decreases relatively linearly with the gap depth. The results of my simulations show that taking the reduction in the magnitude of the torque due to the planetary gaps into account, is one way to potentially solve the problem of too fast migration. This I would argue is the most interesting finding from this project, since the problem of too fast migration has been known for a long time and has no commonly accepted solution.

5.1 Connection to observations

Observations show dark rings in protoplanetary discs at varying distances from the star (see Figure 1.2). Fast migration like in the classical Type-I and Type-II migration picture is a problem when we try to explain these gaps by planet-disc interactions, since it would

be unlikely to capture planets at large distances from the star; the time-scale $a/\dot{a}$ is so short that these planets will migrate on time-scales much shorter than a million years. In order to explain these gaps from planet formation, slow migration or in-situ growth, is thus required. This I can obtain in the model where there is no Type-II migration and the planet migrates under the action of the disc torques, which are reduced due to the opening of the planetary gap (see Figure 4.14). This model is supported by hydrodynamical simulations, which show that the relation between the torque on the planet and the gap depth is essentially linear (Kanagawa et al., 2018).

The gaps seen in observations are often multiple au wide. In order to reproduce such wide gaps using 1-D simulations one would need to take instabilities, wave-propagation and also the back-reaction on the disc into account. The back reaction on the disc is likely also important in 2-D and 3-D simulations. The widening of the planetary gap due to gas accretion onto the planet is an example of a case where the planet affects the evolution of the protoplanetary disc, and the fact that the gap width is an observational property makes it very important to take into account. It should be mentioned here that the observations of protoplanetary discs are taken at mm wavelengths, so it is not the gas content but the content of mm sized dust that is observed. In order to properly compare the gap depths and gap widths from my model with observations one would thus have to include dust dynamics into the model. This is something that I will do in the near future.

One argument for why planet-disc interactions are the likely origin of dark rings in protoplanetary discs, is that they have been shown to be located near ice-lines (Zhang et al., 2015). This matters for planet formation since the formation of planetesimals, which are the building blocks of planets, is very efficient near ice-lines (Ros & Johansen, 2013; Drazkowska & Alibert, 2017; Schoonenberg & Ormel, 2017). If the growth up to pebble isolation mass is rapid, and gas accretion is as efficient as in my models; then a gap which is deep enough to substantially slow down migration would appear quickly, and the planet would remain fairly close to the ice-line.

In order to improve on these results, a more advanced torque prescription that produces similar results in 1-D simulations as in 2-D and 3-D simulations is required. Alternatively, if one could find a simple relation between the pebble isolation mass obtained in my simulations and the ones obtained in 3-D hydrodynamical simulations, one could use that to scale the torque for low mass planets. A 1-D model which reproduces results of 2-D and 3-D hydrodynamical simulations is desirable since it would decrease the amount of computer power needed drastically. It is also necessary if a study of multiple stages of planet formation is ever to be possible.

Bibliography

Alexander, R. D., & Armitage, P. J. 2007, MNRAS, 375, 500

Alexander, R. D., & Armitage, P. J. 2009, ApJ, 704, 989

ALMA Partnership, Brogan, C. L., Pérez, L. M., et al. 2015, ApJ, 808, L3

Armitage, P. J., & Rice, W. K. M. 2005, arXiv:astro-ph/0507492

Bai, X.-N. & Stone, J. M. 2013, ApJ, 769, 76.

Balbus, S. A., & Hawley, J. F. 1991, ApJ, 376, 214

Baruteau, C., & Masset, F. 2008, ApJ, 672, 1054-1067

Baruteau, C., Crida, A., Paardekooper, S.-J., et al. 2014, Protostars and Planets VI, 667

Bitsch, B., Johansen, A., Lambrechts, M., & Morbidelli, A. 2015, A&A, 575, A28

Bitsch, B., Lambrechts, M., & Johansen, A. 2015, A&A, 582, A112

Bitsch, B., Morbidelli, A., Johansen, A., et al. 2018, arXiv:1801.02341

Chandrasekhar, S. 1961, International Series of Monographs on Physics, Oxford: Clarendon, 1961,

Chiang, E. I., & Goldreich, P. 1997, ApJ, 490, 368

D'Alessio, P., Calvet, N., Hartmann, L., Lizano, S., & Cantó, J. 1999, ApJ, 527, 893

D'Angelo, G., & Lubow, S. H. 2010, ApJ, 724, 730

Drazkowska, J. & Alibert, Y. 2017, A&A, 608, A92.

Duffell, P. C., Haiman, Z., MacFadyen, A. I., et al. 2014, ApJ, 792, L10.

Dürmann, C. & Kley, W. 2015, A&A, 574, A52.

Fedele, D., van den Ancker, M. E., Henning, T., et al. 2010, A&A, 510, A72.

Fedele, D., Carney, M., Hogerheijde, M. R., et al. 2017, A&A, 600, A72.

Fedele, D., Tazzari, M., Booth, R., et al. 2018, A&A, 610, A24.

Fressin, F., Torres, G., Charbonneau, D., et al. 2013, ApJ, 766, 81.

Fulton, B. J., Petigura, E. A., Howard, A. W., et al. 2017, AJ, 154, 109.

Gammie, C. F. 1996, ApJ, 457, 355.

Goldreich, P., & Tremaine, S. 1978, ApJ, 222, 850

Goldreich, P., & Tremaine, S. 1979, ApJ, 233, 857

Goldreich, P., & Tremaine, S. 1980, ApJ, 241, 425

Haisch, K. E., Lada, E. A. & Lada, C. J. 2001, ApJ, 553, L153.

Hallam, P. D., & Paardekooper, S.-J. 2017, MNRAS, 469, 3813

Hartmann, L., Calvet, N., Gullbring, E., & D'Alessio, P. 1998, ApJ, 495, 385

Hartmann, L. 2009, Accretion Processes in Star Formation: Second Edition, by Lee Hartmann. ISBN 978-0-521-53199-3. Published by Cambridge University Press, Cambridge, UK, 2009.,

Hayashi, C. 1981, Progress of Theoretical Physics Supplement, 70, 35

Johansen, A., & Lacerda, P. 2010, MNRAS, 404, 475

Johansen, A. & Lambrechts, M. 2017, Annual Review of Earth and Planetary Sciences, 45, 359.

Kanagawa, K. D., Tanaka, H., Muto, T., Tanigawa, T., & Takeuchi, T. 2015, MNRAS, 448, 994

Kanagawa, K. D., Muto, T., Tanaka, H., et al. 2015, ApJ, 806, L15.

Kanagawa, K. D., Tanaka, H. & Szuszkiewicz, E. 2018, ArXiv e-prints , arXiv:1805.11101.

Kley, W., & Crida, A. 2008, A&A, 487, L9

Kley, W., Bitsch, B., & Klahr, H. 2009, A&A, 506, 971

Lambrechts, M., & Johansen, A. 2012, A&A, 544, A32

Lambrechts, M., & Johansen, A. 2014, A&A, 572, A107

Levison, H. F., Thommes, E., & Duncan, M. J. 2010, AJ, 139, 1297

Lin, D. N. C., & Papaloizou, J. 1986a, ApJ, 307, 395

Lin, D. N. C., & Papaloizou, J. 1986, ApJ, 309, 846

Lovelace, R. V. E., Li, H., Colgate, S. A., & Nelson, A. F. 1999, ApJ, 513, 805

Lubow, S. H., & D'Angelo, G. 2006, ApJ, 641, 526

Lynden-Bell, D., & Pringle, J. E. 1974, MNRAS, 168, 603

Lyra, W., Johansen, A., Klahr, H., et al. 2008, A&A, 491, L41.

Machida, M. N., Kokubo, E., Inutsuka, S.-I., & Matsumoto, T. 2010, MNRAS, 405, 1227

Manara, C. F. 2014, Ph.D. Thesis,

Meyer-Vernet, N., & Sicardy, B. 1987, Icarus, 69, 157

Morbidelli, A., & Nesvorny, D. 2012, A&A, 546, A18

Nakagawa, Y., Nakazawa, K. & Hayashi, C. 1981, Icarus, 45, 517.

Okuzumi, S., Momose, M., Sirono, S.-. iti ., et al. 2016, ApJ, 821, 82.

Ormel, C. W., & Klahr, H. H. 2010, A&A, 520, A43

Paardekooper, S.-J., & Mellema, G. 2006, A&A, 459, L17

Paardekooper, S.-J., Baruteau, C., Crida, A., & Kley, W. 2010, MNRAS, 401, 1950

Paardekooper, S.-J., Baruteau, C., & Kley, W. 2011, MNRAS, 410, 293

Papaloizou, J., & Lin, D. N. C. 1984, ApJ, 285, 818

Pinte, C., Dent, W. R. F., Ménard, F., et al. 2016, ApJ, 816, 25.

Piso, A.-M. A., & Youdin, A. N. 2014, ApJ, 786, 21

Pollack, J. B., Hubickyj, O., Bodenheimer, P., et al. 1996, Icarus, 124, 62

Pringle, J. E. 1981, ARA&A, 19, 137

Pringle, J. E., Verbunt, F., & Wade, R. A. 1986, MNRAS, 221, 169

Quillen, A. C., Blackman, E. G., Frank, A., & Varnière, P. 2004, ApJ, 612, L137

Rafikov, R. R. 2004, AJ, 128, 1348

Ros, K. & Johansen, A. 2013, A&A, 552, A137.

Rowan, D., Meschiari, S., Laughlin, G., et al. 2016, ApJ, 817, 104.

Sano, T., Miyama, S. M., Umebayashi, T., et al. 2000, ApJ, 543, 486.

Schoonenberg, D. & Ormel, C. W. 2017, A&A, 602, A21.

Shakura, N. I., & Sunyaev, R. A. 1973, A&A, 24, 337

Sicilia-Aguilar, A., Henning, T. & Hartmann, L. W. 2010, ApJ, 710, 597.

Tanigawa, T. & Tanaka, H. 2016, ApJ, 823, 48.

Tanigawa, T. & Watanabe, S.-. ichiro . 2002, ApJ, 580, 506.

Turner, N. J., Fromang, S., Gammie, C., et al. 2014, Protostars and Planets VI, 411.

Umebayashi, T. & Nakano, T. 1988, Progress of Theoretical Physics Supplement, 96, 151.

Vigan, A., Bonavita, M., Biller, B., et al. 2017, A&A, 603, A3.

Ward, W. R. 1997, Icarus, 126, 261

Zhang, K., Blake, G. A., & Bergin, E. A. 2015, ApJ, 806, L7